Quaternary Science Reviews 304 (2023) 107994

Contents lists available at ScienceDirect

Quaternary Science Reviews

journal homepage: www.elsevier.com/locate/quascirev

Nonlinear rainfall effects on savanna fire activity across the African Humid Period

Allison T. Karp [a, b, *], Kevin T. Uno [c], Melissa A. Berke [d], James M. Russell [b], Christopher A. Scholz [e], Jennifer R. Marlon [f], J. Tyler Faith [g, h, i], A. Carla Staver [a, j]

[a] Department of Ecology and Evolutionary Biology, Yale University, New Haven, CT, 0651, USA
[b] Department of Environmental, Earth and Planetary Sciences, Brown University, Providence, RI, 02912, USA
[c] Division of Biology and Paleo Environment, Lamont-Doherty Earth Observatory of Columbia University, Palisades, NY, 10964, USA
[d] Department of Civil & Environmental Engineering & Earth Sciences, University of Notre Dame, Notre Dame, IN, 46556, USA
[e] Department of Earth and Environmental Sciences, Syracuse University, Syracuse, NY, 13244, USA
[f] Yale School of the Environment, Yale University, New Haven, CT, 06511, USA
[g] Natural History Museum of Utah, University of Utah, Salt Lake City, UT, 81408, USA
[h] Department of Anthropology, University of Utah, Salt Lake City, UT, 84112, USA
[i] Origins Centre, University of the Witwatersrand, Johannesburg, South Africa
[j] Yale Institute of Biospheric Studies, Yale University, New Haven, CT, 06511, USA

ARTICLE INFO

Article history:
Received 30 November 2022
Received in revised form
1 February 2023
Accepted 2 February 2023
Available online xxx

Handling Editor: Mira Matthews

Keywords:
Holocene
Paleoclimatology
Paleofire
Africa
Organic geochemistry
Continental biomarkers
Vegetation dynamics

ABSTRACT

Fire is a key ecosystem process in tropical and subtropical savannas, with a varying role that depends on hydroclimate but also on feedbacks between fire and vegetation. In savannas, fire response to changes in rainfall depends on mean annual rainfall: in arid and semi-arid systems, burned area increases as rainfall increases fuel amount, whereas in mesic systems with high fuel moisture, burned area decreases as rainfall increases. The non-linear relationship between burned area and rainfall may be due in part to changes in the constraints on fire activity that shift the limiting factor for burning in savannas from fuel amount to fuel moisture with increasing rainfall and decreasing seasonality. Vegetation-fire feedbacks can also promote a shift from fire-prone savanna vegetation to forest taxa that suppress fire as rainfall increases. However, modern observations are, by definition, constrained to short-term dynamics, and the longer-term effects of precipitation changes on fire activity have not been evaluated. These longer-term impacts are especially relevant for evaluating biome transitions changing in response to variable hydroclimate and fire activity. The Late Pleistocene and early Holocene African Humid Period (AHP; ~14.5 −5.5 ka), when rainfall increased substantially across northern and equatorial Africa, provides an opportunity to examine long-term fire responses to increased precipitation at sites with different mean annual rainfall amounts. Here, we combine new polycyclic aromatic hydrocarbons (PAHs) records of paleofire activity at two East African lake basins (Lakes Victoria and Turkana) with previously published fire records (i.e., charcoal, levoglucosan) at five sites (GeoB7920-2, GeoB9508-5, Lakes Chala, Tanganyika and Bosumtwe) to examine responses of fire activity along a rainfall gradient (from <200 mm to 1500 mm). Our synthesis reveals fire dynamics that are consistent with modern ecosystem dynamics and shows that fire activity at each site followed predicted patterns across the AHP depending on initial mean rainfall, with increased fire activity at arid to semi-arid sites and decreased fire activity at mesic-to-humid sites. Results illustrate that fire responses to hydroclimate are nonlinear, such that the same direction of change in precipitation can elicit different fire responses depending on the total precipitation at a site. Accounting for heterogeneity in hydroclimate, even within biomes, may improve predictions of how fire activity will respond to future changes in rainfall regimes.

1. Introduction

Tropical and subtropical grasslands and savannas cover ~25% of

Abbreviations: AHP, African Humid Period; PAH, Polycyclic aromatic hydrocarbon; MAP, Mean Annual Precipitation.

* Corresponding author. Department of Ecology and Evolutionary Biology, Yale University, New Haven, CT, 0651, USA.
E-mail address: Allison.karp@yale.edu (A.T. Karp).

https://doi.org/10.1016/j.quascirev.2023.107994
0277-3791/

the earth's terrestrial surface, but they are responsible for >80% of global annual burned area, with the largest contribution from Africa (Giglio et al., 2006; Strömberg and Staver, 2022; Van Der Werf et al., 2017). To better constrain the role of fire in global carbon budgets, we must understand how African savanna fire activity will respond to projected climate changes, and especially precipitation changes, on multiple time scales. In the coming decades, rainfall patterns across Africa are predicted to shift substantially (Dunning et al., 2018; Haile et al., 2020; Rowell et al., 2015), and in grassy systems, fire spread depends on fuel-load (the amount of fuel) and fuel-moisture (if the fuel is dry enough to ignite), both of which depend on rainfall (He and Lamont, 2017). Yet, global fire history analyses included limited data from grasslands (Leys et al., 2018; Marlon et al., 2016) and primarily focus on the effects of temperature on fire activity rather than rainfall (Marlon et al., 2008; Daniau et al., 2012).

Today, African savannas are distributed across an extensive rainfall gradient (200–2000 mm yr^{-1}) (Aleman et al., 2020; Staver et al., 2011a), and fire response to changes in rainfall depend on the initial hydroclimate conditions (i.e., mean annual precipitation; MAP). In general, burned area increases as rainfall increases in arid regions and burned area decreases as rainfall increases in mesic regions (Alvarado et al., 2020). Potential rainfall thresholds between fuel-load limited (fire increases with increasing rainfall) and fuel-moisture limited (fire decreases with increasing rainfall) savannas, and between fire-maintained savanna and forest ecosystems, have been identified spatially using remote sensing products (Alvarado et al., 2020; Staver et al., 2011b). However, evidence that sites transition across these fire thresholds in response to long-term changes in rainfall remains elusive, potentially because the temporal extent of present-day observations is very limited.

Examining paleofire activity on millennial timescales remedies this limitation by allowing us to test how savanna fire dynamics respond to large rainfall changes during periods of Quaternary climate change. The most recent prolonged interval of wet conditions, the so-called “African Humid Period” (AHP; ~14.5–5.5 ka) was characterized by an average 280 ± 138 mm yr^{-1} increase in rainfall across many sites in sub-tropical and tropical Africa (Holmes and Hoelzmann, 2017) in response to shifts in insolation (deMenocal et al., 2000; Tierney et al., 2011b). This interval provides an exceptional opportunity to examine how savanna fire activity responded to similar changes in precipitation at different sites along the rainfall gradient. Several studies have examined Holocene pollen and phytolith records to identify transitions between savanna and forest (e.g., Aleman et al., 2020; Phelps et al., 2020), and other studies have examined late Holocene charcoal records to identify fuel-load limited and fuel-moisture limited fire regimes (Colombaroli et al., 2014). However, very few studies have explicitly compared changes in savanna fire activity at separate sites during an interval of pronounced rainfall change (but see Moore et al., 2022; Urban et al., 2015).

If both fuel amount and fuel moisture limit paleofire activity, savanna fire responses should be dependent on initial hydroclimate conditions. We can make predictions about fire during the AHP informed by modern work. Today, in arid to semi-arid savannas (0–700 mm yr^{-1}), fire activity is limited by the amount of grass-fuel available to burn (fuel-load limited). Grass biomass increases in response to increasing rainfall (Sala et al., 2012), so interannual fire activity in these arid savannas has a strong positive correlation with total rainfall amount (Alvarado et al., 2020; Archibald et al., 2009). In addition to changes in MAP, the seasonality of rainfall can also impact fuel-load dynamics. In fuel-load limited systems, increased growing season length (i.e., decreased rainfall seasonality) also adds to grassy fuel loads and promotes overall fire spread (Kahiu and Hanan, 2018; Mondal and Sukumar, 2016). If these modern processes operate on long time-scales, we predict that fire activity at arid to semi-arid sites will increase with increasing rainfall (or decreased seasonality) during the AHP, then decrease with decreasing rainfall in the late Holocene (Fig. 1a) (Archibald et al., 2009; Staver et al., 2017).

In contrast, in semi-mesic savannas (700–1000 mm yr^{-1}), fuel needs to dry out enough to allow fire to ignite and spread, so fire activity may instead be limited by fuel moisture content (fuel-moisture limited) (Krawchuk and Moritz, 2011). In fuel-moisture limited systems, interannual fire activity is negatively correlated with rainfall, with higher fire following drought years (Alvarado et al., 2020; Aragão et al., 2008) and in longer dry seasons (Mondal and Sukumar, 2016). These dynamics mean that at mesic sites, there are two potential hypotheses for how fire might respond to increased rainfall during the AHP. Either (1) fire activity will display the same patterns predicted at semi-arid sites (Fig. 1a), indicating fuel-load-limited responses to rainfall (Archibald et al., 2009), or (2) fire activity will initially increase with rainfall and then start to decrease with continued increases in rainfall (Fig. 1b), indicating a transition from fuel-load to fuel-moisture limitation (Alvarado et al., 2020).

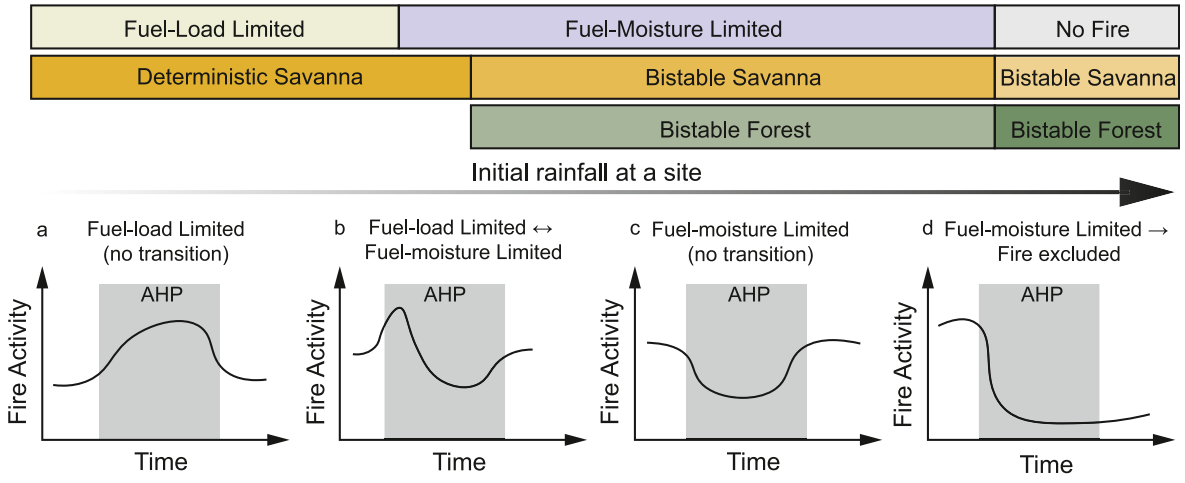

Fig. 1. Hypotheses of fire response to increasing then decreasing rainfall over the AHP. a) Expectations for sites that are fuel-load limited and remain fuel-load limited. b) Expectations for sites that transition from fuel-load limited to fuel-moisture limited, then back. c) Expectations for sites that are fuel-moisture limited and remain fuel-moisture limited. d) Expectations for sites that are fuel-moisture limited savannas that transition to fire-excluded forests.

In mesic savannas (1000–2000 mm yr^{-1}), the relationship between fire, fuels, and rainfall is further complicated because reductions in grassy fire activity can transition a savanna to a forest (Staver et al., 2011a). In fuel-moisture limited systems, reductions in dry season length have a strong impact of drying of fuels and fire spread (Kahiu and Hanan, 2018; Mondal and Sukumar, 2016). Seasonality decreases in fuel-moisture limited systems not only limit fire activity, but can exclude it completely (Archibald et al., 2009). Thus, reduced seasonality is more likely to favor forests at the expense of savannas than increases in MAP alone (Aleman et al., 2020; Staver et al., 2011b). Once the system is forested, fire activity might be less responsive to rainfall decreases at the end of the AHP, because of a stabilizing feedback between moist-closed canopy taxa that inhibits fire (Hoffmann et al., 2012; Pausas and Bond, 2020). Therefore, at mesic sites, there are also two potential hypotheses for fire responses to changes in rainfall during the AHP. Either (1) fire activity will decrease with increasing rainfall, then increase with decreasing rainfall (Fig. 1c), indicating the site is fuel-moisture-limited (Alvarado et al., 2020) or (2) fire will not just decrease, but will be fully suppressed as rainfall increases (Fig. 1d), leading to forest transitions if crossing a savanna-forest threshold. This last scenario would specifically result from decreasing seasonality (or more rainfall in the dry season), which is necessary to exclude fire (Archibald et al., 2009) to enable savanna-forest transitions.

To test these predictions, we will examine fire, hydroclimate, and vegetation records (new and from the literature) from sites that span the AHP (Berke et al., 2012; Dupont and Schefuβ, 2018; Ivory and Russell, 2016; Moore et al., 2022; Morrissey and Scholz, 2014; Nelson et al., 2012; Niedermeyer et al., 2010; Shanahan et al., 2016;

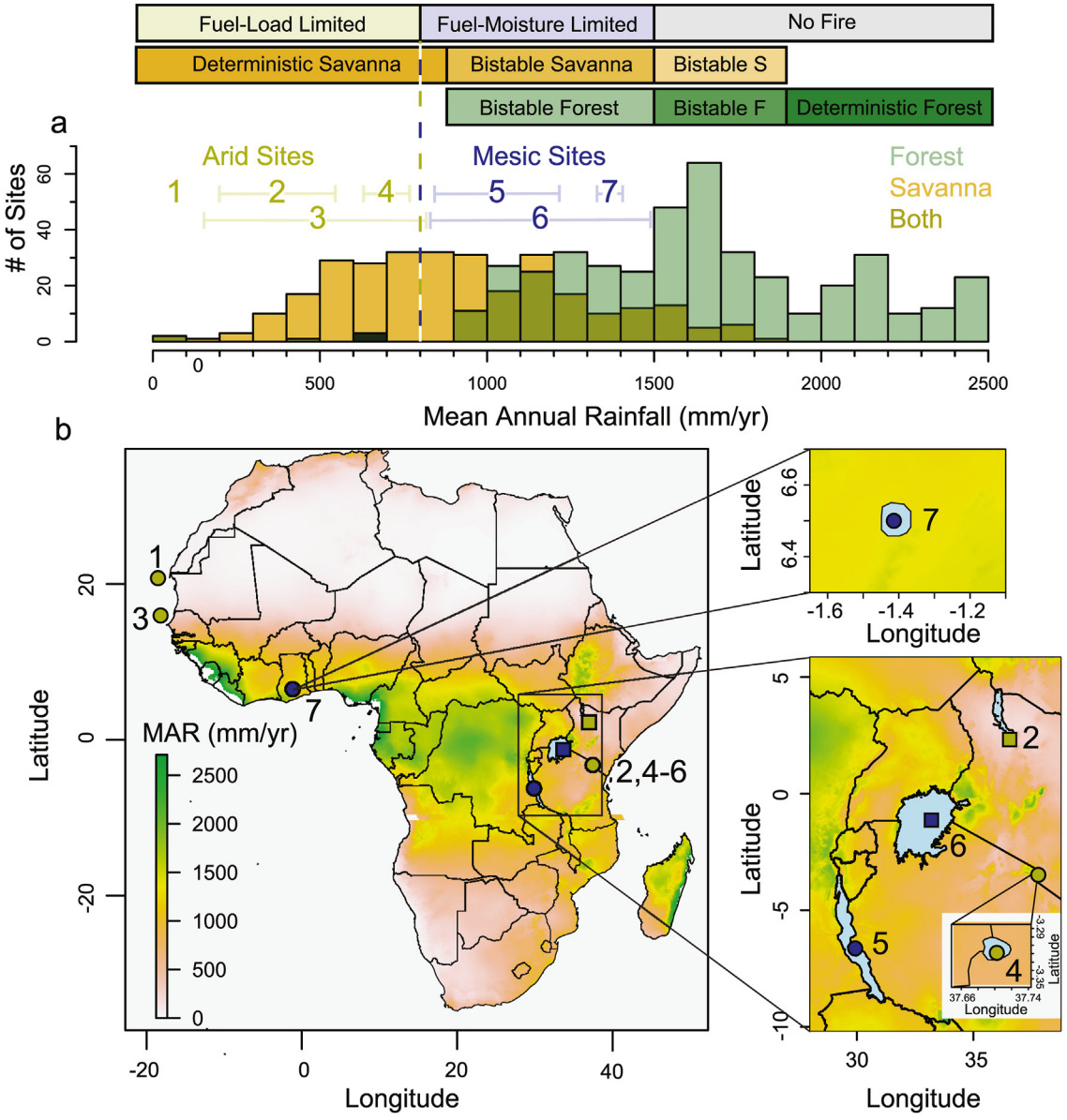

Fig. 2. Distribution of sites across the modern savanna rainfall gradient. a) Modern savanna and forest distribution along the mean annual rainfall gradient defined using data from modern Africa floral survey sites replotted from Aleman et al. (2020). Threshold from fuel-load limited to fuel moisture limited (yellow blue line) defined from Alvarado et al. (2020). Numbers correspond to sites in (b). Blue points and numbers are sites on the mesic side of the rainfall gradient, and yellow points and numbers are sites on the arid side of the rainfall gradient. b) Map of sites discussed in this study. Sites marked with circles have previously published records of fire activity, sites marked with squares are new fire records generated in this study. 1) GeoB7920 2) Lake Turkana 3) GeoB9508 4) Lake Chala 5) Lake Tanganyika 6) Lake Victoria 7) Lake Bosumtwe. MAR data is from Fick and Hijmans (2017), error bars are standard deviation across the hydrologic basins.

Tierney et al., 2008, 2011b) (Fig. 2). In order to characterize AHP fire activity patterns, we contribute two new fire records using polycyclic aromatic hydrocarbons (PAHs) from lakes with previous organic geochemistry reconstructions of hydrologic change during the AHP (Berke et al., 2012; Morrissey, 2014): Lake Turkana and Lake Victoria. This results in a total of seven sites along the African savanna rainfall gradient (<100–1500 mm yr^{-1}).

2. Hydroclimate context and site selection

2.1. The African Humid Period (AHP)

The Late Pleistocene and early Holocene African Humid Period (AHP; ~14.5–5.5 Ka) corresponds with increased rainfall across much of northern and tropical Africa (deMenocal et al., 2000). This increase in rainfall was driven by increased Northern Hemisphere summer insolation associated with minimum precession. The resulting shifts in the North African monsoon, the tropical rain belt, and other oceanic and atmospheric circulation patterns increased precipitation across a broad swath of northern and equatorial Africa (deMenocal et al., 2000; Kutzbach and Street-Perrott, 1985; Shanahan et al., 2015). Complementary lines of empirical evidence support increased water availability during the AHP at sites across Northern, Eastern, and Southern Africa, including dust flux records, δ^2H of leaf waxes, pollen, and lake level reconstructions (summarized in Shanahan et al., 2015). However, while ~100 distinct sites record signals of the AHP, the timing and magnitude of the event varied depending on site and region (Shanahan et al., 2015; Tierney et al., 2011a). The termination of the AHP was both temporally and spatially transgressive, occurring progressively later at lower latitudes as the extent of the tropical rain belt collapsed towards the equator (Shanahan et al., 2015). Additionally, in many cases, the increasingly wet conditions of the AHP were interrupted by a brief hiatus associated with the Younger Dryas stadial (12.7–11.3 ka), which is apparent in proxy records as abrupt reversals or plateaus in wetting trends (Berke et al., 2014; Holmes and Hoelzmann, 2017; Shanahan et al., 2016; Tierney et al., 2011b, 2017). Due to this heterogeneity, the timing of hydroclimate change at individual sites must be empirically constrained in order to examine the effect this event had on local ecology. We selected sites with existing records of leaf wax δ^2H and use these records to define the beginning and end of the AHP at each site (Table 1). This facilitates analysis of the timing of changes in fire relative to changes in precipitation regimes during the AHP.

2.2. Site summary

Here we assess fire dynamics at seven sites across a modern rainfall gradient (Fig. 2). Half of the sites are currently arid to semi-arid (~100–600 mm yr^{-1}; GeoB7920, Turkana, GeoB9508, Chala) and the other half are mesic (~1000–1500 mm yr^{-1}; Tanganyika, Victoria, Bosumtwe) (Fig. 2) (Fick and Hijmans, 2017). Sites are numbered in Fig. 2 in order of increasing rainfall, with all modern rainfall extracted from an annual sum of the WorldClim monthly precipitation product for the hydrologic basins for 5 lakes and the Senegal River basin for GeoB9508-5 (Fick and Hijmans, 2017); note that rainfall has been estimated for the entire hydrologic basin of each study site, not for the lake or site itself.

Previously published sites were selected if they 1) covered the correct time interval (late Pleistocene through the Holocene), 2) had a leaf wax hydrogen isotope record indicating that rainfall increased during this interval, and thus, could be used to define the timing of the AHP at the specific site, and 3) had a paleofire record from the same core (charcoal or organic fire markers). Five sites fit this criteria —GeoB7920-2, GeoB9508-5, Chala, Tanganyika, Bosumtwe) (Dupont and Schefuβ, 2018; Ivory and Russell, 2016; Moore et al., 2022; Nelson et al., 2012; Niedermeyer et al., 2010; Shanahan et al., 2016; Tierney et al., 2008). All proxies are described in more detail below. Core GeoB7920-2 (#1 in Fig. 2) is a marine site off the coast of Mauritania that captures the greening of the Sahara during the AHP and is our most arid site. Core GeoB9508-5 (#3 in Fig. 2) is a marine site of the coast of Senegal which captures a signal from the Sahel, a region that today experiences 492 ± 352 mm yr^{-1} rainfall (Moore et al., 2022; Niedermeyer et al., 2010). Lake Chala (#4 in Fig. 2) is a crater lake in Kenya, and the surrounding area currently receives an average of 747 ± 42 mm yr^{-1} of rainfall (Nelson et al., 2012; Tierney et al., 2011a). Lake Tanganyika (#5 in Fig. 2) is a rift basin lake in East Africa and receives an average of 1054 ± 172 mm yr^{-1} of rainfall (Ivory and Russell, 2016; Tierney et al., 2008). Lake Bosumtwe (#7 in Fig. 2) is a crater lake in Ghana, which currently experiences 1390 ± 29 mm yr^{-1} of rainfall (Shanahan et al., 2015, 2016).

The remaining two sites (Lakes Turkana and Victoria) have records of hydroclimate (leaf wax δ^2H), but no directly associated records of fire activity. We generated new fire activity records from these sites from polycyclic aromatic hydrocarbons (PAHs) in archived organic extracts. Lake Turkana (#2 in Fig. 2) is the largest rift basin lake in the eastern branch of the East Africa Rift System and has an average of 468 ± 273 mm yr^{-1} of rainfall in the basin,

Table 1
Rainfall constraints for all AHP fire sites. Modern rainfall estimates extracted from Fick and Hijmans (2017). Method and citations correspond to reconstructed maximum AHP rainfall estimates.

Site	AHP Timing (Defined by leaf wax δ^2H)	Modern Rainfall in hydrologic basin	Max AHP Rainfall	Method	Citation
Core GeoB7920-2	11.3–5.0 ka	<100 mm yr^{-1}	300–700 mm yr^{-1} Median = 800 mm yr^{-1} (300–1700 mm yr^{-1})	Pollen δ^2H Modeling	Peyron et al. (2006) Tierney et al. (2017)
Lake Turkana	13.8–5.5 ka	468 ± 273 mm yr^{-1}	560–660 mm yr^{-1}	Lake Balance Modeling	(Fischer et al., 2020; Junginger and Trauth, 2013)
Core GeoB9508-5	15.0–4.8 ka	492 ± 352 mm yr^{-1}	700–1000 mm yr^{-1}	Vegetation modeling	Larrasoaña et al. (2013)
Lake Chala	11.3–4.8 ka	747 ± 42 mm yr^{-1}	?	–	–
Lake Tanganyika	15.0–4.5 ka	1054 ± 172 mm yr^{-1}	1400 mm yr^{-1}	δ^2H Modeling scaled to pollen	Tierney et al. (2010)
Lake Victoria	11.3–4.8 ka	1185 ± 321 mm yr^{-1}	1500–2000 mm yr^{-1} (Lake Edwards)	Pollen	Beuning and Russell (2004)
			1375–1564 mm yr^{-1} (Lake Naivasha)	Lake Balance Modeling	Bergner et al. (2003)
Lake Bosumtwe	15.1–3.2 ka	1390 ± 29 mm yr^{-1}	1480–1900 mm yr^{-1}	Pollen Lake Balance Modeling	(Peyron et al., 2006; Shanahan et al. (2008)

and Lake Victoria (#6 in Fig. 2) is the largest lake in East Africa and receives an average of 1185 ± 321 mm yr^{-1} of rainfall (Berke et al., 2012; Morrissey and Scholz, 2014).

2.3. Leaf wax δ^2H as a hydroclimate proxy

Shifts in hydroclimate are often constrained using leaf wax δ^2H records. In the tropics, relative shifts in leaf wax δ^2H are usually interpreted as changes in rainfall because at low latitudes the amount of incoming precipitation is generally the main control on environmental δ^2H (Dansgaard, 1964; Rozanski et al., 1993). This can be complicated by other factors that can impose second-order controls on leaf wax δ^2H, including the effects of changes in moisture source that influence the δ^2H of rainfall (Konecky et al., 2019; Moore et al., 2014), changes in plant growth season, etc. (Collins et al., 2013; Sachse et al., 2012; Tipple et al., 2013). These effects complicate quantitative reconstructions of rainfall change from leaf wax δ^2H. However, qualitative interpretations about the magnitude and direction of rainfall change across these sites are possible by making some reasonable assumptions. Firstly, δ^2H values before the AHP were generally slightly enriched or similar to the modern values at all the of sites (Berke et al., 2012; Dupont and Schefuβ, 2018; Morrissey, 2014; Niedermeyer et al., 2010; Shanahan et al., 2015; Tierney et al., 2008, 2011b). We infer that pre-AHP rainfall was either similar or slightly more arid than what is recorded at sites today. Secondly, all sites feature negative shifts in δ^2H values during the AHP relative to pre- and post-AHP (Berke et al., 2012; Dupont and Schefuβ, 2018; Morrissey, 2014; Niedermeyer et al., 2010; Shanahan et al., 2015; Tierney et al., 2008, 2011b). While the influence of source water and seasonality on δ^2H may differ slightly at some sites (e.g., Lake Chala; Tierney et al., 2011b), we assume these ^2H depletions indicate increased rainfall amount relative to modern conditions during the AHP at each site. This is additionally supported by independent estimates for rainfall increases at many of the selected sites (Table 1). We use these estimates to anchor our predictions of fire response based on projected magnitude of rainfall increases.

We address how the size of these shifts may have differed between sites and how other complicating hydroclimate factors may impact δ^2H records in more detail in Section 5. However, based on available data it is reasonable to conclude that all sites examined here experienced wetter conditions than the present during the AHP, and thus can be used to test fire response to a similar long-term rainfall shift across sites with different initial hydroclimate contexts.

3. Materials and methods

3.1. Core descriptions and age models for newly generated PAH records

3.1.1. Lake Victoria

Core V95−1 P was collected with a Kullenberg piston corer in 1995 from the north-central portion of the lake in water depth of 68 m as part of the International Decade of East African Lakes (IDEAL) program (Fig. 2). V95−1 P was subsampled for organic geochemical analyses at an average sampling resolution of ~250 years (Berke et al., 2012). The age model is based on radiocarbon dates of the 20−70 mm fraction of pollen-lignin-charcoal from Johnson et al. (2000) and of bulk organic carbon and wood fragments from Berke et al. (2012). We updated the previous age model, which was based on linear interpolation, using the flexible, Bayesian age-depth program "rbacon" and the IntCal20 calibration (Blaauw and Christeny, 2011) (Fig. S1).

3.1.2. Lake Turkana

Three cores (Turk10−4 P, Turk10−14 P, and Turk10−46 P) were collected using a Kullenberg piston corer in 2010 from the South Basin of Lake Turkana in water depths of 52, 56, and 58 m, respectively (Fig. 2). The three cores were stratigraphically correlated using magnetic susceptibility, gamma ray density, total organic carbon content, and high-resolution seismic-stratigraphic data, and together provide a continuous composite sediment record (Morrissey and Scholz, 2014). The cores were subsampled at an interval of ~240 years. The age model was previously published in Morrissey and Scholz (2014) and is based on 24 radiocarbon dates from bulk organic matter of mixed lacustrine and terrestrial origin, bulk carbonate mud, discrete macrophyte specimens, or ostracod and gastropod shells. The age model for the composite core record was generated using a flexible, Bayesian age-depth program, "Bacon" (Blaauw and Christeny, 2011).

3.2. Sediment extraction and preparation

For Turkana and Victoria cores, PAHs were measured from archived lipid extracts that had previously been analyzed for other classes of compounds (plant waxes, GDGTs; Berke et al., 2012; Morrissey et al., 2018). For Lake Victoria samples, freeze-dried, homogenized sediment was extracted using soxhlet extraction with 2:1 dichloromethane:methanol (DCM:MeOH) for 24 h to produce a total lipid extract (TLE) (Berke et al., 2012). For Lake Turkana Samples, freeze-dried and homogenized sediment samples were extracted using DIONEX™ accelerated solvent extraction with dichloromethane (DCM:Methanol (9:1) (Morrissey et al., 2018). The polar and apolar fractions of lipid extracts were then separated using activated alumina columns, with Hexane:DCM (9:1) DCM:Methanol (1:1) as eluents. A 1,1′-binaphthyl recovery standard was added to the total lipid extract (TLE) splits from Lake Victoria samples and apolar fractions from Lake Turkana samples, which were then dried gently under pure N_2 gas, then separated into aploar, aromatic, and polar classes by silica-gel column chromatography (Polissar et al., 2019; Wakeham and Pease, 2004).

3.3. PAH quantification

PAHs were characterized and quantified using an Agilent GC-MSD. Samples were dissolved in toluene and injected in splitless mode into an inlet with a single-taper glass liner with a deactivated glass wool plug connected to a 30 m × 0.25 mm inner diameter column with a 0.25 μm thick HP-5ms stationary phase. The oven was set to 90 °C (1.5 min hold) then ramped to 150 °C at 15 °C/min, then to 320 °C at 4 °C/min. Samples were run in a hybrid SIM/Scan mode, where the MSD rapidly alternates between selective ion monitoring (SIM) and full scan collections over the course of a single run (Karp et al., 2021c). The 50-ms dwell time in SIM mode on target PAH ions enables us to make high sensitivity and accurate measurements of PAHs. The PAHs are first characterized and identified from full scan data by matching fragmentation patterns and retention times to a 17 PAH authentic standard suite (Restek SV Calibration Mix #5 combined with retene and 1,1′-binaphthyl), then quantified with the SIM data. A 5-point calibration curve of for each PAH in the standard suite was established every 10 to 15 samples to ensure ion currents represented a linear response to PAHs. Concentrations for all PAH were calculated relative to the peak area of an internal standard (1,1′-binaphthyl) and response factors from analyses of standards.

Previous studies have normalized PAHs to a plant biomarker to account for changes in overall plant biomass and preservation (Denis et al., 2017; Karp et al., 2018, 2021c). However, given that we are explicitly examining potential transitions between fuel-load

driven fire regimes to fuel-moisture driven fire regimes, this normalization has the potential to mask trends driven by rainfall-dependent increases in fuel loads. Instead, we examine sedimentary fluxes of PAHs, calculated from the sedimentation rates from the age model. This allows us to place these sites into context of those that use sedimentary charcoal fluxes as a fire proxy. To account for potential shifts in organic preservation that may impact these fluxes we also normalize PAHs to total organic carbon (TOC) concentrations. TOC values were extracted from previous publications (Cockerton et al., 2015; Morrissey and Scholz, 2014) using WebPlotDigitizer.

3.4. Statistics

3.4.1. PAH source corrections and ratios

PAHs can be sourced from fire and from other processes that are not pyrogenic, which can confound paleofire interpretations (Stogiannidis and Laane, 2015; Wakeham et al., 1980). However, the relative distributions of alkylated homologs of phenanthrene (P = phenanthrene, MP = methylated phenanthrene, DMP = demethylated phenanthrene, TMP = trimethylated phenanthrene) can be used to identify PAHs from pyrogenic versus non-pyrogenic inputs (Fig. 3A) (Stogiannidis and Laane, 2015). Because alkylated forms are not favored in fast, high temperature reactions (Blumer and Youngblood, 1975; Stogiannidis and Laane, 2015), burn products are dominated by parent forms (P > MP > DMP > TMP) (Karp et al., 2020; Stogiannidis and Laane, 2015). However, alkylated PAHs are favored by slow heating, such as the sedimentary maturation of organic matter (Blumer and Youngblood, 1975; Stogiannidis and Laane, 2015), so methyl and dimethyl forms dominate (P<MP≈DMP>TMP) (Karp et al., 2021c).

Here we use non-negative matrix factorization (NMF) to identify and quantify relative contributions of PAH sources in each sample after Karp et al. (2021a, 2021c). NMF deconstructs or 'unmixes' a multidimensional dataset to identify endmember distributions (Lee and Seung, 2001). NMF was conducted in R with the package 'NMF' and the Euclidian distance method from Lee and Seung (2001) (Core, 2019; Gaujoux and Seoighe, 2010). Before using PAHs to make paleofire interpretations, PAH concentrations were corrected by multiplying by the "pyrogenic factor abundance" reconstructed using NMF for each sample (Fig. 3) (Karp et al., 2021a, 2021c). Samples with <10% of pyrogenic inputs were excluded from interpretations of paleofire (2 samples from Victoria, 5 samples from Turkana).

PAH size is related to physiochemical properties that control compound partitioning in the environment (Jenkins et al., 1996; Lima et al., 2005). Examining PAH ratios of the smaller compounds (LMW = sum of phenanthrene, anthracene, fluoranthene and pyrene) over the sum of all the parent PAHs measured may reflect differences in contributions from smoke/aeolian derived PAHs (higher LMW/Total ratios) and residue/fluvially transported PAHs (lower LMW/Total ratios) (Karp et al., 2020).

3.4.2. Correlations and significance test

All statistical analyses were conducted in R (Core, 2019). Kruskal-Wallis tests were used to evaluate if PAH size and retene distributions differed significantly between the lakes, as well as during the AHP relative to before and after (Hollander and Wolfe, 1973). To access relationships between NMF endmembers, PAHs, and plant biomarkers, we evaluated the Pearson Coefficient correlations (Pearson, 1948). This was calculated using the surrogateCor function from the Astrochron package in R (Meyers, 2014). To account for temporal autocorrelation this function uses the Ebisuzaki method for serially correlated data and a Bayesian Monte Carlo approach to calculate a significance level (Ebisuzaki, 1997).

4. Results

4.1. New PAH records from Victoria and Turkana

NMF models at both lakes explained greater than 99% of variance in PAHs. NMF of methylated phenanthrenes reveals that both lakes have substantial non-pyrogenic contributions (Fig. 3). At Turkana, the best fit NMF with meaningful endmembers identified three sources: petrogenic, pyrogenic, and weathered/gymnosperm (Fig. 3a). There are no directional trends in source patterns through time, but uncorrected PAH concentrations are most strongly correlated with the pyrogenic endmember ($\rho = 0.52$, $p = 0.01$; Fig. 4a). At Victoria, the best fit NMF with meaningful endmembers identified two sources: petrogenic and pyrogenic (Fig. 3b). Pyrogenic inputs generally decrease through time (Fig. 3b), which parallels an overall increase in uncorrected PAH concentrations ($\rho = 0.44$, $p = 0.08$; Fig. 4b). The NMF correction method using the pyrogenic endmember allows us to make interpretations of fire dynamics that are not confounded by shifts in petrogenic carbon dynamics through time (Karp et al., 2021a, 2021c).

PAH size distributions varied between sites (Vic LMW/Total $\mu = 0.44$, Turk LMW/Total $\mu = 0.68$; $N_{Turk} = 54$, $N_{Vic} = 30$, $\chi^2 = 36.751$, $p \ll 0.001$) (Fig. 5), and there is a slight but significant decrease (~0.08) in the LMW/total values during the AHP at both lakes (Turk: $N_{AHP} = 27$, $N_{pre\&post\ AHP} = 27$, $\chi^2 = 3.4957$, $p = 0.06$; Vic: $N_{AHP} = 12$, $N_{pre\&post\ AHP} = 19$, $\chi^2 = 3.7895$, $p = 0.05$). PAH flux and leaf wax δ^2H records from Turkana and Victoria are moderately but not significantly correlated over the last 20 ka (Turk $\rho = -0.40$, $p = 0.022$ and Vic $\rho = -0.60$, $p = 0.138$). While this indicates that wetter samples may be weakly tied to higher fire at both lakes, the trends across the overall wetter AHP diverge between the lakes. Although PAH records at both lakes have high variability, distinctive larger patterns emerge. At Turkana (semi-arid), PAHs initially increase then decrease over the AHP (Fig. 6c), while at Victoria (mesic), PAHs decrease progressively over the AHP (Fig. 6g).

PAH fluxes and TOC normalized concentrations both increase at Turkana and decrease at Victoria (Fig. 6), which indicates that PAH fluxes are not greatly impacted by preservation issues in the sediments. However, there are some slight differences in the timing and relative magnitude of trends of these two PAH metrics at Victoria (Fig. 6e; Fig. 6g). The decrease in PAHs over the AHP is more abrupt in the PAH/TOC record than in the PAH flux record. Additionally, PAH/TOC values increase slightly in the late Holocene after the AHP, while flux values stay low. Here we use PAH flux records from Turkana and Victoria for comparison to fire activity records from other AHP sites around Africa because all previously published fire proxies are expressed in terms of flux ($cm^{-2}\ yr^{-1}$).

We examine co-occurring fire marker concentrations and plant biomarker concentrations to distinguish between sites that are fuel-load versus fuel-moisture controlled. The plant biomarker, β-amyrin derivative (1,2,3,4-tetrahydro-2,2,9-tri-methylpicene), is an angiosperm biomarker (Simoneit, 1986) with an aromatic chemical structure and has been used when normalizing PAHs to a plant biomarker (Denis et al., 2017; Karp et al., 2021c). While this normalization was not used here (see Methods), PAH concentrations are highly correlated to β-amyrin derivative ($\rho = 0.74$, $p < 0.01$) at Lake Turkana, but show no correlation at Lake Victoria ($\rho = -0.13$, $p = 0.476$) (Fig. 4).

To assess softwood burning and identify conifer contributions to sedimentary records (Miller et al., 2017; Simoneit, 1977), we use retene, which is a functionalized PAH derived from conifer resins. Because retene is a byproduct of both conifer resin degradation and softwood burning (Simoneit, 2002; Wakeham et al., 1980), a ratio of Ret/3-ring = retene/(retene + phenanthrene + anthracene) is preferred to identify PAH fire records with substantial conifer

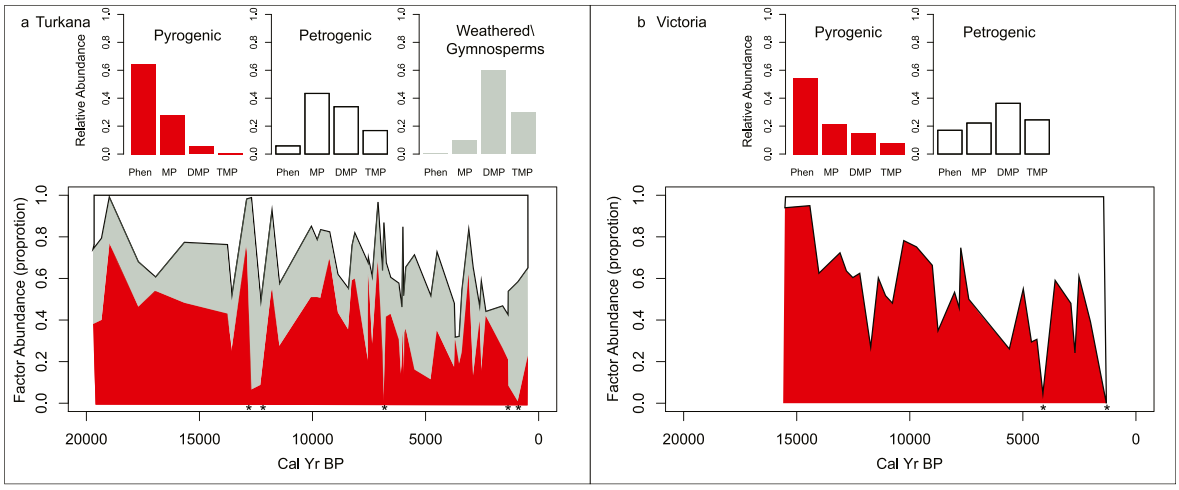

Fig. 3. NMF of alkylated Phenanthrenes to constrain PAH source inputs. Reconstructed end-members (bar plots) and relative factor abundance for each sample (plots through time) are shown for each of the lakes. a) NMF results for Lake Turkana b) NMF results for Lake Victoria. Asterisks mark samples that have <10% pyrogenic and were excluded from paleofire interpretations.

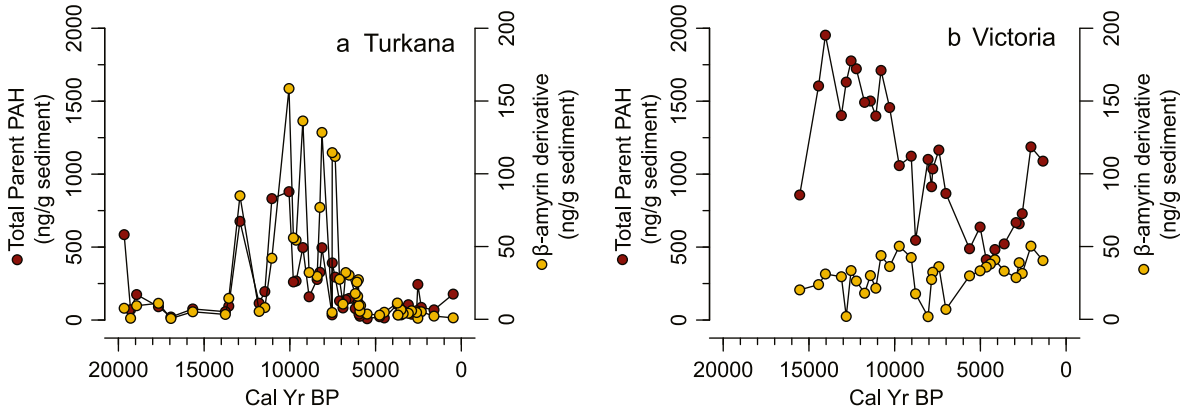

Fig. 4. PAH and β-amyrin derivative concentrations at Lake Turkana (a) and Lake Victoria (b). PAH concentrations are in red and β-amyrin derivative concentrations are in gold.

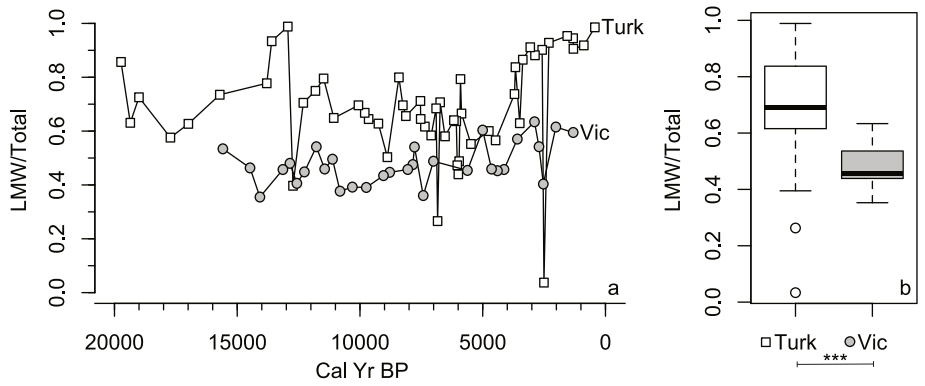

Fig. 5. LMW/Total PAH ratios from Lake Turkana (white) and Lake Victoria (grey). A) LMW/Total ratios through time B) Box and whisker plots of LMW/Total values between both lakes. Asterisks represent significance (<0.001) from a Kruskal-Wilcox test for difference between sets of samples ($p = 1.3 \times 10^{-9}$).

sources (Karp et al., 2020). Ret/3-ring ratios at Lake Turkana are generally fairly low, but highly variable ($\mu = 0.22 \pm 0.19$) (Fig. 7a). Ret/3-ring values at Victoria are significantly less than those at Lake Turkana ($N_{Turk} = 54$, $N_{Vic} = 30$, $\chi^2 = 34.677$, $p \ll 0.001$), and consistently low ($\mu = 0.06 \pm 0.03$) (Fig. 7a).

4.2. Previously published fire records

We briefly report trends from previously published fire records that we use in section 5 to make interpretations about fire activity over the greater savanna rainfall gradient. Because we define the timing of the AHP at each site based on the individual δ^2H records,

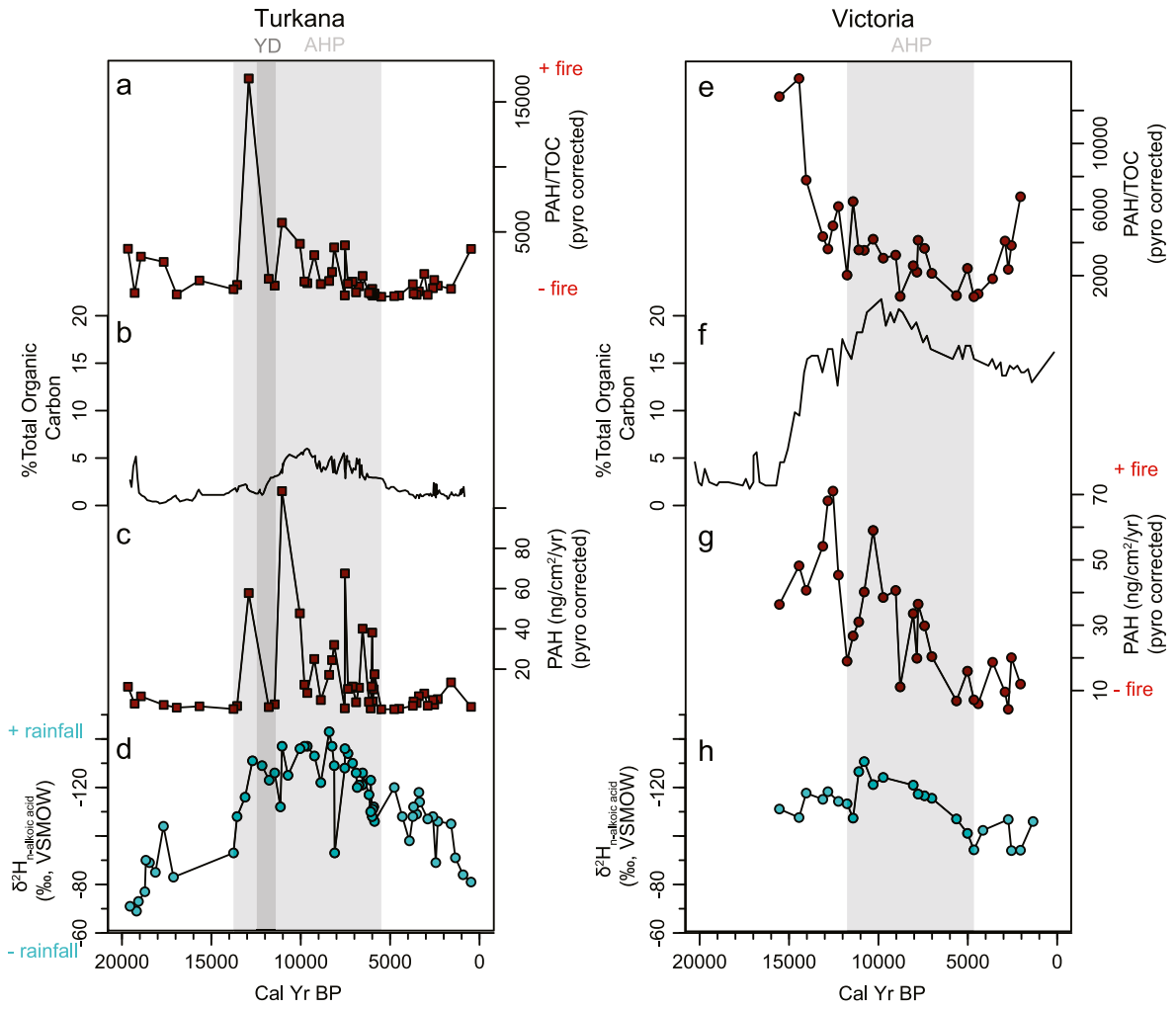

Fig. 6. Fire and hydroclimate during the AHP at Lake Turkana and Lake Victoria. All PAH records have been corrected using NMF pyrogenic abundance. a) Total Parent PAHs normalized to TOC at Lake Turkana b) % TOC at Lake Turkana (Morrissey and Scholz, 2014). c) Total Parent PAHs flux at Lake Turkana. d) Leaf wax Hydrogen isotopes at Lake Turkana (Morrissey, 2014). e) Total Parent PAHs normalized to TOC at Lake Victoria f) % TOC at Lake Victoria (Cockerton et al., 2015). g) Total Parent PAHs flux at Lake Victoria. h) Leaf wax Hydrogen isotopes at Lake Victoria (Berke et al., 2012).

the dates used for the start and end of the AHP in the following discussion are different for each site (Table 1). We describe site results in order from most arid to most humid. At GeoB7920-2 (Fig. 2, Site #1) we first converted char accumulation (particles/cm^3) to charcoal flux (particles/cm^2/yr) using the sedimentation rates from the age model (Dupont and Schefuβ, 2018). Charcoal flux first increased then decreased during the AHP (11.3–5.0 ka) (Fig. 8b) (Dupont and Schefuβ, 2018). At GeoB9508-5 (Fig. 2, Site #3), charcoal flux initially increased at the start of the AHP (15–12.7ka), decreased by an order of magnitude after the Younger Dryas (Fig. 8e) (Moore et al., 2022), and then remained stable through the rest of the AHP (11.3–4.8 ka) (Fig. 8e) (Moore et al., 2022). At Lake Chala (Fig. 2, Site #4), charcoal flux was high in the late Pleistocene (>14 ka) then decreased during the Pleistocene to Holocene transition (14–11.3 ka) (Fig. 8h) (Nelson et al., 2012). During the AHP (11.3–4.8 ka) charcoal fluxes at Lake Chala increased slightly, then decreased after 4.8 ka (Fig. 8h) (Nelson et al., 2012). At Lake Tanganyika (Fig. 2, Site #5), charcoal flux increased at the onset of the AHP (15.0 ka) then little to no charcoal was deposited at the site after the Younger Dryas (<11.5 ka) (Fig. 9b) (Ivory and Russell, 2016). Finally, at Lake Bosumtwe (Fig. 2, Site #7), levoglucosan (another class of fire marker) flux decreased precipitously at the AHP onset (15.1 ka) before dropping to zero during the middle of the AHP (11.5–6 ka) (Fig. 9h) (Shanahan et al., 2016).

5. Discussion

In section 5.1, we discuss how PAH transport and sourcing processes inform interpretations of paleofire shifts at Lakes Turkana and Victoria. We then interpret fire response to increased AHP rainfall at each of the seven sites, moving along the rainfall gradient from arid (Section 5.2) to humid (Section 5.3). In section 5.4, we synthesize how fire regimes responded to the AHP through both time and space. We find that sites displayed distinct fire responses during the AHP consistent with predictions based on modern empirical and theoretical work (Fig. 1). We find strong evidence that fire dynamics depend on initial hydroclimate conditions at a site, and that several sites exhibit distinct fire dynamics when switching between biomes. Finally, we consider how other variables changing during the AHP besides mean annual precipitation may complicate savanna fire response (Section 5.5), and we integrate their effects into this interpretive framework.

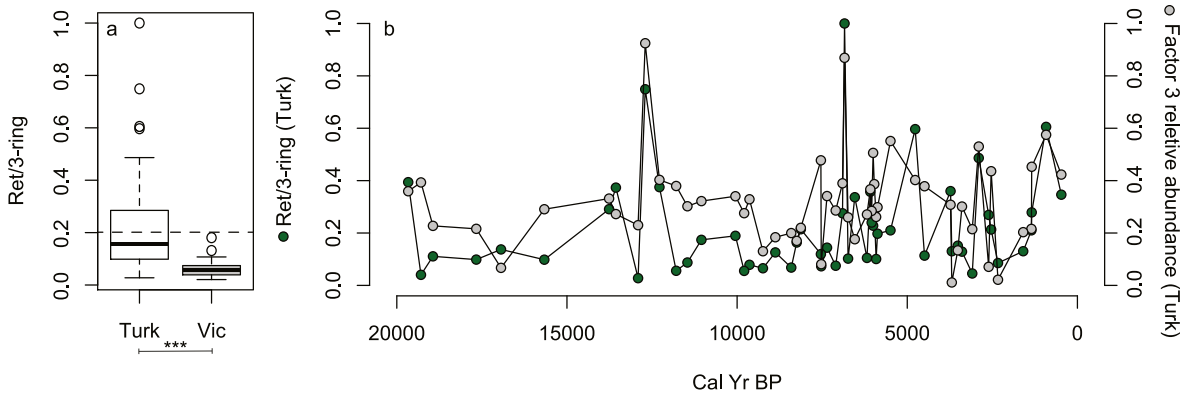

Fig. 7. Retene/3-ring PAH ratios. a) Box and whisker plots of Ret/3-ring values between both lakes: Lake Turkana (white) and Lake Victoria (grey). Asterisks represent significance (<0.001) from a Kruskal-Wilcox test for difference between sets of samples ($p = 1.3 \times 10^{-9}$). b) Ret/3-ring ratios and the conifer/weathered factor (Fig. 3a, grey factor 3) abundance through time. Both datasets are from Lake Turkana. The strong correlation between Ret/3-ring and NMF factor 3 ($\rho = 0.71$, $p < 0.01$) supports the interpretation that factor 3 is coming from a gymnosperm source.

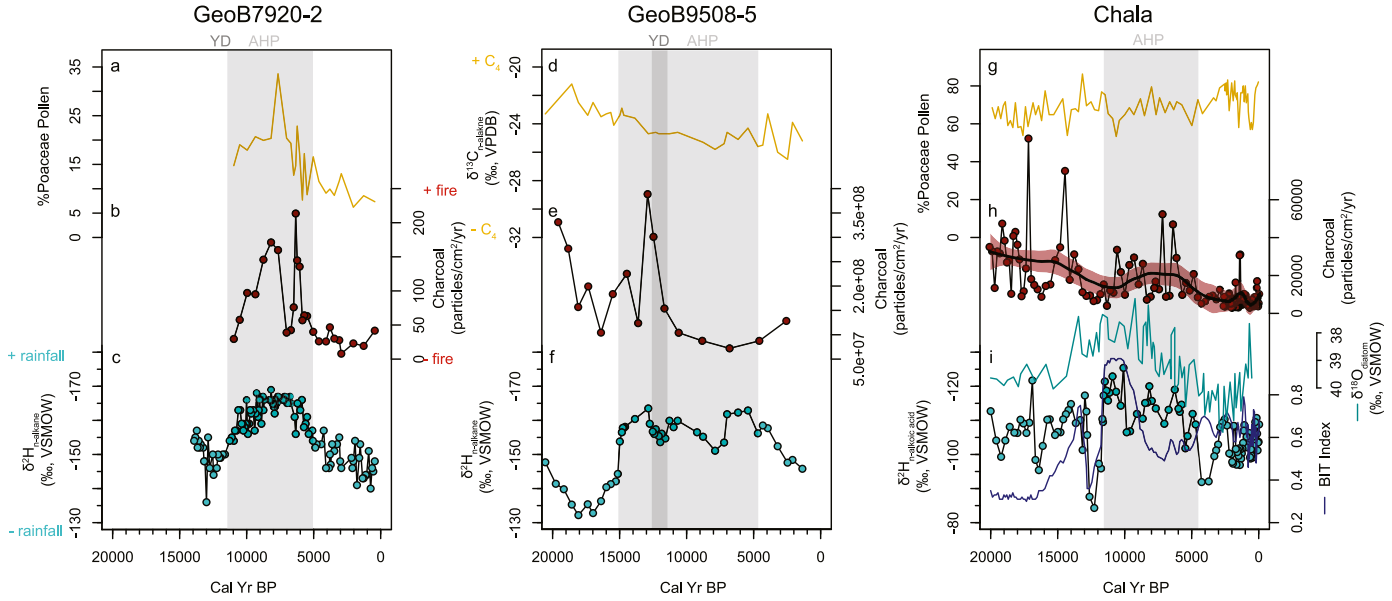

Fig. 8. Fire and hydroclimate during the AHP at previously published semi-arid sites: GeoB7920-2, GeoB9508-3, and Lake Chala. a) Percent grass pollen at GeoB7920-2 (Dupont and Schefuβ, 2018) b) Charcoal flux at GeoB7920 (Dupont and Schefuβ, 2018). c) Leaf wax δ^2H (C_{31} *n*-alkane) at GeoB7920 (Dupont and Schefuβ, 2018). d) Leaf wax $\delta^{13}C$ (C_{31} *n*-alkane) at Geob9508 (Niedermeyer et al., 2010) e) Charcoal flux at GeoB9508 (Moore et al., 2022) f) Leaf wax δ^2H (C_{31} *n*-alkane) at GeoB9508-5 (Niedermeyer et al., 2010) g) Percent grass pollen (van Geel et al., 2011) at Lake Chala. h) Charcoal flux at Lake Chala (Nelson et al., 2012). To highlight general trends in a high variability dataset, we smoothed charcoal flux with 'loess' using a 0.3 span. The shaded region is the 97.5% confidence interval. i) Hydroclimate proxies at Lake Chala. Teal points are leaf wax δ^2H (C_{28} fatty acid) (Tierney et al., 2011a), solid dark blue line is BIT index (Verschuren et al., 2009), and solid teal line is $\delta^{18}O_{diatom}$ (Barker et al., 2011).

5.1. PAH transport and sourcing

The distinct PAH size distributions between the lakes (higher LMW/Total at Turkana and lower LMW/Total at Victoria) match what we would expect based on differences in sedimentary transport processes (Fig. 5). Lake Victoria has 25 inflowing tributaries that deliver water and sediment to the basin (Sene and Plinston, 1994), so we expect PAHs were transported via both aeolian and fluvial transport. However, Turkana's main inflowing rivers are the Omo, which contributes to the northern basin, and the Turkwel and Kerio Rivers which flow into the central part of the lake. Aeolian sediment transport is more pronounced in the southern basin where the cores were acquired, compared to the central and northern part of the lake (Morrissey and Scholz, 2014; Yuretich, 1986).

Despite these basin-scale differences, both settings do show a similar though small decrease (~0.08) in LMW/Total ratios during the AHP (Fig. 5b). During this time, precipitation and presumably runoff increased at both lakes (Garcin et al., 2012; Morrissey and Scholz, 2014; Talbot and Lærdal, 2000), which would have likely increased the contribution of fluvially transported PAHs to the sediment. Despite this commonality, the lakes show divergent PAH patterns through the AHP (Fig. 6b and f). Therefore, shifts in transport mechanism are unlikely to obscure our interpretations of fire history or account for differences in fire history between the lakes.

While both lakes had petrogenic PAH inputs (Fig. 3), the NMF correction method allowed for the identification and exclusion of these confounding PAH sources to support our paleofire interpretations. Curiously, in addition to a petrogenic and pyrogenic sources, Lake Turkana also had a third meaningful source end-member whose features that resemble either a weathered PAH

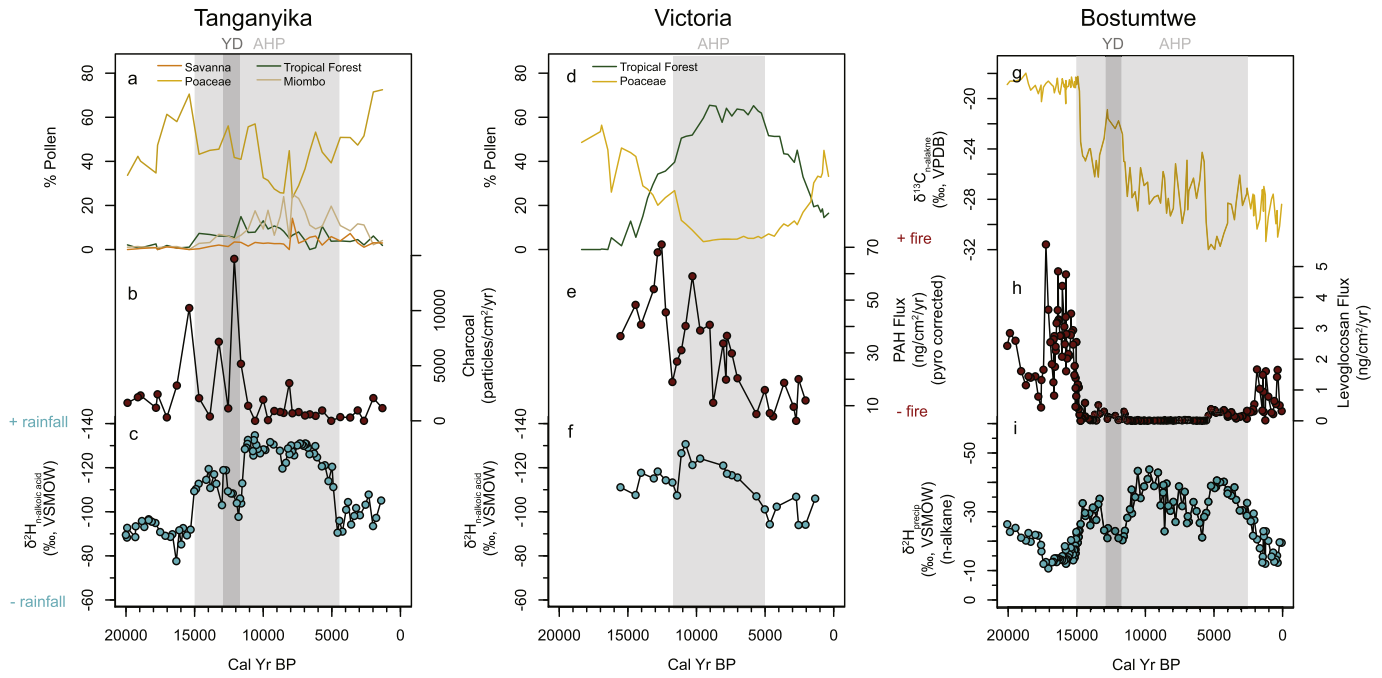

Fig. 9. Vegetation, fire and hydroclimate during the AHP at mesic sites: Lake Tanganyika, Lake Victoria, and Lake Bosumtwe. a) Pollen type percentages at Lake Tanganyika (Ivory and Russell, 2016). Tropical Forest = Moraceae, Macaranga-type, *Celtis*, and *Trema orientalis*-type, Miombo = *Brachystegia*, *Isoberlinia*, and *Uapaca*, Savanna = *Acacia*, *Commiphora africana*-type, and Combretaceae undifferentiated b) Charcoal flux at Lake Tanganyika (Ivory and Russell, 2016). c) Leaf wax δ^2H (C_{28} *n*-alkanoic acid) at Lake Tanganyika (Tierney et al., 2008). d) Pollen type percentages at Lake Victoria (Kendall, 1969). Tropical Forest = Moraceae, Urticaceae, *Trema*, *Macaranga*, and *Celtis*. e) PAH flux at Lake Victoria. f) Leaf wax δ^2H (C_{28} *n*-alkanoic acid) at Lake Victoria (Berke et al., 2012). g) Leaf wax $\delta^{13}C$ (C_{31} n-alkane) at Lake Bosumtwe (Shanahan et al., 2015, 2016). h) Levoglucosan flux at Lake Bosumtwe (Shanahan et al., 2016). i) Estimated precipitation calculated from leaf wax δ^2H (C_{31} *n*-alkane) at Lake Bosumtwe (Shanahan et al., 2015, 2016).

source or PAH contributions specifically from gymnosperm/conifers. PAHs that have been degraded by microbes in soils and sediments display a distinctive increasing staircase distribution of methylated phenanthrenes (P < MP < DMP < TMP) (Mallick et al., 2011; Stogiannidis and Laane, 2015). Although the third endmember generally displays this weathering pattern (Fig. 3a), it is interrupted by maximum of DMPs (P<MP<DMP>TMP), and this most closely resembles the alkylated phenanthrene distribution burn products of some, but not all, gymnosperm taxa (Karp et al., 2020; Simoneit, 2002; Yunker et al., 2002).

Retene patterns at Lake Turkana support the interpretation that this endmember may reflect distinct conifer/gymnosperm inputs to the PAH record. While Ret/3-ring ratios at Lake Turkana were generally low ($\mu = 0.22$) (Fig. 7a); they were highly correlated with the abundance of the third NMF endmember ($\rho = 0.71$, $p < 0.01$) (Fig. 7b) and inversely correlated with the pyrogenic component ($\rho = -0.65$, $p < 0.01$). Importantly, Ret/3-ring was not significantly correlated to the petrogenic endmember ($\rho = 0.03$, $p = 0.80$), which indicated that the relationship between Ret/3-ring and the other two endmembers was not simply a relic of the abundances of the factors summing to one, but rather represented a meaningful indication of a tradeoff between gymnosperm and angiosperm pyrogenic PAH inputs. It is possible these are inputs from the Ethiopian highlands to the North of Lake Turkana, which include *Afrocarpus*, an endemic conifer (Adie and Lawes, 2011).

This pattern of a distinct gymnosperm source is consistent with a basin that is severely fuel limited. If savanna fire activity was low, fire inputs from very distal gymnosperm taxa likely contributed more to the record than they would in another context where fires were not fuel-load limited. These taxa likely burned very infrequently (or not at all), but if grass-derived fire activity was also low, distal conifer inputs may have been a significant source of PAHs, and therefore, contributed to PAH inputs. However, we note that since we correct PAH concentrations to the pyrogenic NMF factor, we can be confident that interpretations of PAH records reflect savanna fire response to the AHP rather than shifts in distal conifer burning.

Because Lake Victoria is relatively mesic, we hypothesize that retene patterns at Victoria would be distinct from Turkana because PAH fluxes indicate fire activity was 1) likely higher and 2) likely fuel-moisture, rather than fuel-load, limited (i.e., there is usually enough fuel to burn) (Figs. 4 and 6C, G), such that pyrogenic PAHs and non-petrogenic PAHs overall were likely dominated by savanna burning inputs. And indeed, at Victoria, Ret/3-ring values were significantly less than those at Lake Turkana ($N_{Turk} = 54$, $N_{Vic} = 30$, $\chi^2 = 34.677$, $p \ll 0.001$) and were consistently below the threshold of conifer inputs (Fig. 7a) ($\mu = 0.06$, all<0.2) (Karp et al., 2020). Together this indicates that fire-derived PAHs at Victoria were dominated by angiosperms. Additionally, the best-fit NMF at Victoria does not include an endmember dominated by DMPs, which defines the conifer (gymno)/weathered factor. Together PAH, DMP, and retene patterns at both lakes indicate the pyrogenic NMF component of the PAHs (and therefore the corrected fluxes) reflects burning of savannas, rather than distal gymnosperm forests, which is consistent with the strong connections between frequent grass-fueled fires and savannas in modern day subtropical systems (Murphy et al., 2019; Staver et al., 2011b).

5.2. Fire regimes at arid to semi-arid savanna sites

We hypothesized that fire activity at the arid and semi-arid sites along the savanna rainfall gradient would be fuel-load limited, and thus that fire activity would increase as rainfall increased during the AHP (see Fig. 1).

Core GeoB7920-2 (Fig. 2, Site #1) is a marine site off the coast of Mauritania that records the greening of the Sahara during the AHP

(Fig. 2; Dupont and Schefuβ, 2018; Nelson et al., 2012; Tierney et al., 2011b). Rainfall at this latitude (~20°N) would have increased substantially from <100 mm yr^{-1} to between 300 and 800 mm yr^{-1} during the AHP (Table 1) (Peyron et al., 2006; Tierney et al., 2017), moving from a fireless desert system into a fuel-load limited semi-arid savanna (Dupont and Schefuβ, 2018). Therefore, we expect fire activity to track increases in rainfall during the AHP (Fig. 1a). Charcoal patterns at GeoB7920 indicate fire activity was high during the AHP, but dropped precipitously as rainfall decreased at the termination of the event (Dupont and Schefuβ, 2018) (Fig. 8b), fitting our expectations for a fuel-load limited system. Pollen records from the site indicate high contributions of grasses and savanna woody vegetation during the AHP, which declined as desertification occurred at the termination of the AHP (Dupont and Schefuβ, 2018) (Fig. 8a). These dynamics are consistent with expectations for fire responses to increased rainfall in an arid region, where fuel-loads are limiting (Fig. 1a).

The Omo-Turkana Basin (Fig. 2, Site #2) sits on the semi-arid side of the savanna rainfall gradient (468 ± 273 mm yr^{-1}). Precipitation is estimated to have increased to ~560–660 mm yr^{-1} during the peak of the AHP (Table 1) (Fischer et al., 2020; Junginger and Trauth, 2013). In Africa today, the rainfall threshold from fuel-load limited to moisture-load limited fire regimes is ~800 mm yr^{-1} (Alvarado et al., 2020), so we can conservatively predict that the system should remain fuel-load limited and that fire activity should increase during the wetter AHP (Fig. 1a). And indeed, PAH patterns at Lake Turkana indicate that AHP fire activity was elevated (Fig. 6c), likely as a result of increased grass production accompanying increased rainfall (Sala et al., 2012). This interpretation of the site as fuel-load limited is further supported by strong correlations between β-amyrin derivative and PAHs fluxes at the site ($\rho = 0.74$, $p < 0.01$) (Fig. 4a), indicating that PAH concentrations are tightly coupled to fuel loads. Again, these dynamics are consistent with expectations for fire responses to increased rainfall in a semi-arid region, where fuel-loads are limiting (Fig. 1a).

Core GeoB9508-5 (Fig. 2, Site #3) captures a signal from the Sahel. Today, this region experiences on average 492 mm yr^{-1} rainfall, and, based on vegetation modeling, rainfall likely increased to 700–1000 mm yr^{-1} during the AHP (Larrasoaña et al., 2013; Niedermeyer et al., 2010) (Table 1). Because this projected AHP rainfall range brackets the modern rainfall threshold between fuel-load limited and moisture-load limited fire regimes (~800 mm yr^{-1}; Alvarado et al., 2020), this increase may have shifted the fuel dynamics at the site from fuel-load limited to moisture-load limited. If this was the case, we predict fire activity would have initially increased with rainfall, then started to decrease while AHP rainfall remained high (Fig. 1b). Charcoal patterns and the δ^2H record at GeoB9508 confirm these expectations. Initially, the charcoal flux mirrors the δ^2H record, pre-AHP fire activity decreased as rainfall decreased, and then, at the start of the AHP, fire activity increased as rainfall increased (Fig. 8e and f) (Moore et al., 2022; Niedermeyer et al., 2010). Subsequently, during the middle of the AHP, charcoal flux decreased though δ^2H indicates rainfall was still high (Fig. 8e and f). Despite the relative decrease in fire activity from the start of the AHP, substantial charcoal inputs ($>5 \times 10^7$ particles $cm^{-1}yr^{-1}$), combined with higher leaf wax carbon isotope values (>-26‰), indicate the site remained a fire-prone, C_4-dominated savanna throughout the AHP (Fig. 8d and e) (Moore et al., 2022). Together, this evidence is consistent with the modern observation that fire activity is highest in moisture-limited mesic savannas (800–1200 mm yr^{-1}) (Archibald and Hempson, 2016; Moore et al., 2022; Van Der Werf et al., 2008). Overall, GeoB9508 displays dynamics of savanna that transitioned from fuel-load to fuel-moisture limitation of fire activity (Fig. 1b).

Lake Chala (Fig. 2, Site #4) is a crater lake in Kenya which currently experiences 747 ± 42 mm yr^{-1} of rainfall (Fig. 2). Chala approaches the modern fuel-load/fuel-moisture limited threshold (800 mm yr^{-1}) (Alvarado et al., 2020), so could conceivable display fuel-load limited behavior, fuel-moisture limited behavior, or a transition between the two. Chala is a complicated site to interpret for several reasons. Firstly, though the Lake Chala fatty acid δ^2H are more negative during the AHP, the magnitude of this shift is very small (only about −5‰; Fig. 8i) compared to other sites (−15 to −40‰; Fig. 6d; Fig. 6h; Fig. 8c; Fig. 8f; Fig. 9c; Fig. 9i). This could indicate that influences besides the amount effect, such as shifts in seasonal source water (Tierney et al., 2011b) or mixing of fatty acid derived from terrestrial and aquatic sources to the lake sediment (van Bree et al., 2018), obscured rainfall shifts. Alternatively, the δ^2H record could indicate there was not a substantial shift in rainfall during the AHP. Additionally, another organic hydroclimate proxy record at Chala, the Branched/Isoprenoidal Tetraethers (BIT) Index, tracks the δ^2H record from 20–10 ka, but diverges after 9 ka (Fig. 9i) (Tierney et al., 2011b). The BIT was initially interpreted as a proxy for runoff based on the assumption that branched GDGTs are produced in soils (Hopmans et al., 2004), but in Lake Chala, branched GDGTs are also produced *in situ* (Buckles et al., 2014; Sinninghe Damsté et al., 2012), meaning shifts in BIT values do not necessarily record shifts in rainfall and runoff. Finally, $\delta^{18}O_{diatom}$, interpreted to record P-E balance of the lake, indicate either more rainfall or reduced evaporation during the AHP (11.3–4.8 ka) (Barker et al., 2011). Ultimately, it is likely that rainfall did increase during the AHP at the site, but that this was a relativity small shift.

Fire patterns across the AHP are muted at Chala (Fig. 9h). Charcoal flux was variable in the late Pleistocene (20–15 ka), low during the Younger Dryas (12.7–11.3 ka), then was moderate during the AHP (11.3–4.8 ka) (Nelson et al., 2012). Despite the complexities in interpreting these proxies at the site, fire trends seem to better track AHP leaf wax δ^2H and $\delta^{18}O_{diatom}$ than BIT values, with higher fire during negative δ^2H and $\delta^{18}O_{diatom}$ periods, and decreases in fire activity coinciding with δ^2H and $\delta^{18}O_{diatom}$ increases (Fig. 8h; Fig. 8i) (Barker et al., 2011; Nelson et al., 2012). The decrease in fire at the YD (which all proxies indicate was dry) combined with the slight increase in fire during the AHP is consistent with a fuel-load limited site that remains close to the threshold but does not transition to fuel-moisture limitation (Fig. 8h; Fig. 8i). At a fuel-load limited site, we expect charcoal flux to track the amount of grass (i.e., fuel) on the landscape. Pollen records indicate grasses dominated the vegetation surrounding Chala (>60% grass) throughout the entire record (Fig. 8g) (van Geel et al., 2011), and $\delta^{13}C$ of charcoal indicate burning was generally dominated by C_4 grass inputs (Blaauw et al., 2011). We note that there are not substantial increases in grass pollen during the AHP at Chala (Fig. 8g; Fig. 8h). Unlike pollen concentration data, pollen percentage records capture relative vegetation shifts, rather than the amount of biomass on a landscape. Because this site remains grass dominated, a lack of relationship between δ^2H and grass pollen does not rule out an increase in fuel loads in response to rainfall. However, the very slight increase in charcoal does suggest if the site was fuel limited, then this limitation was not very strong. In savannas today, the strength of the dominant correlation between fire and rainfall (either positive or negative) weakens at sites close to the rainfall boundary between fuel-load or fuel-moisture limited systems (Alvarado et al., 2020). Thus, the very slight increase in AHP fire at Chala could be 1) because the site is at the very high end of the fuel-load limited range, thus not strongly dependent on fuel loads, 2) due to a very slight change in rainfall at the site, or 3) a combination of both. Because we are unsure by how much rainfall increased during the AHP, we cautiously interpret fire dynamics as fuel-load limited at Chala. We note that because of the uncertainties at this site, we do not include the site in our synthesis

(Fig. 11), which summarizes the sites in relation to our hypotheses (Fig. 1).

5.3. Fire regimes at semi-mesic to mesic savanna sites

We hypothesized that fire activity at the semi-mesic to mesic sites along the savanna rainfall gradient would be generally fuel-moisture limited, and thus that fire activity would decrease as rainfall increased during the AHP. In the extreme, this decrease could cause fire to mostly disappear from a system, which we expect might additionally complicate dynamics at the highest rainfall sites. The suppression of fire can trigger a transition from savanna to humid forest, which might not be reversed at the end of the AHP, if savanna and forest are indeed maintained by fire as alternative stable states (Staver et al., 2011a).

Lake Tanganyika (Fig. 2, Site #5) has an average of 1054 ± 172 mm yr^{-1} of rainfall in the basin (Ivory and Russell, 2016; Tierney et al., 2008). Rainfall estimates based on scaling the δ^2H shifts to LGM-modern changes in precipitation estimated from pollen, indicate an increase to ~1400 mm yr^{-1} during the AHP (Tierney et al., 2010). Given current rainfall is above the modern fuel-load/fuel-moisture limited threshold (800 mm yr^{-1}) (Alvarado et al., 2020), we predicted that fire decreased and then increased across the AHP as rainfall increased and then decreased (Fig. 1c). The reality is more complicated than this: Tanganyika charcoal fluxes indicate high and variable fire activity coincided with increasingly wet conditions at the beginning of the AHP (15.0 ka), then fire activity abruptly decreased following the Younger Dryas (12.7–11.5 ka) as rainfall increased further during the middle of the AHP (Fig. 9b and c) (Ivory and Russell, 2016). This pattern suggests that fire activity at the site was initially fuel-load limited, transitioning to a fuel-moisture limited fire regime during the AHP (Fig. 1b). That this site was initially fuel load limited is somewhat surprising given modern rainfall at Tanganyika, which substantially exceeds the modern fuel-load/fuel-moisture threshold (Alvarado et al., 2020). There are three possible explanations: either 1) deglacial rainfall at the site was less than 800 mm yr^{-1}, 2) the rainfall threshold between fuel-load and fuel-moisture limited savannas was higher during the terminal Pleistocene than today due to differences in precipitation minus evaporation (P-E), or 3) changes in rainfall seasonality during the AHP influenced fire activity. There is support for either the first or third possibility. Pollen-based precipitation estimates support the first, lower rainfall possibility: estimates place LGM rainfall between 720 and 896 mm yr^{-1}, which straddles the 800 mm yr^{-1} fire threshold (Bonnefille and Chalie, 2000; Tierney et al., 2010; Vincens et al., 1993). Modeling work across the AHP at Tanganyika generally supports the third, seasonality possibility: an increase in moisture from the Atlantic during the dry season and/or "short rains" may have resulted in reduced seasonality during the AHP thereby decreasing fire after the Younger Dryas (Tierney et al., 2010, 2011a). The decrease in AHP fire activity is accompanied by a decrease in grass pollen, and an increase in *miombo* woodland taxa (Fig. 9a). These changes in both fire activity and vegetation structure persist even after the termination of the AHP, suggesting that a shift among multiple stable states occurred (probably savanna to woodland or dry forest). Overall, Tanganyika displays dynamics of a site transitioning not just from fuel-load to fuel-moisture limitation (Fig. 1b), but also to a dry-forest stable state (Fig. 1d). Observations remain conceptually consistent with predictions based on modern savanna fuel and fire dynamics, but also emphasize the strong role of seasonality.

The Lake Victoria basin (Fig. 2, Site #6) is mesic (1185 ± 321 mm yr^{-1}). While there are currently no estimates for the exact magnitude of the AHP rainfall increase at Victoria, rainfall at Lakes Edward and Naivasha, which bracket the basin to the East and West, is estimated to have increased to 1300–2000 mm yr^{-1} during the AHP (Table 1) (Bergner et al., 2003; Berke et al., 2012; Beuning and Russell, 2004). The site is currently above the modern fuel-load/fuel-moisture limited threshold (800 mm yr^{-1}) (Alvarado et al., 2020), and we therefore expect that fire activity decreased with increased rainfall during the AHP (Fig. 1c). The ecological dynamics at this site also make it a good candidate for complications from changing biome composition, since it currently sits within the savanna-forest bistable zone (700–1900 mm yr^{-1}) (Fig. 2a) (Aleman et al., 2020) and might have experienced a potentially irreversible shift from savanna to forest with decreased fire activity (Fig. 1d). PAH fluxes at Lake Victoria suggest that fire activity decreased during the AHP (Fig. 9e), with no correlation between β-amyrin derivative and PAHs concentrations ($\rho = -0.13$, $p = 0.476$) (Fig. 4b). Both of these lines of evidence support the interpretation that the site experienced increasing fuel-moisture limitation of fire activity during the AHP (11.3–4.8 ka) (Fig. 1c and d). Recently, Temoltzin-Loranca et al. (2023) published charcoal records from three new cores taken from Lake Victoria. In all three records charcoal fluxes also decreased during the AHP (Temoltzin-Loranca et al., 2023), providing additional confidence that fire activity around Lake Victoria decreased in response to increasing fuel-moisture limitation.

The PAH and charcoal records from Lake Victoria differ at the end of the AHP (6–4 ka). The PAH record indicates fire activity remained low (Fig. 9e), but the charcoal records indicate a peak between 5–4 ka (Temoltzin-Loranca et al., 2023). Among the potential taphonomic explanations for this discrepancy (e.g., different transport pathways or source areas (Vachula et al., 2022; Vachula and Richter, 2017)), one plausible candidate is that large macroscopic charcoal, such as that analyzed at Lake Victoria (>200 μm) (Temoltzin-Loranca et al., 2023), may be biased towards woody burning (Leys et al., 2017). Indeed, Temoltzin-Loranca et al. (2023) link this charcoal increase to the expansion of *Podocarpus-Juniperus* forests. Though Ret/3-ring ratios indicate PAHs are not sourced predominately from gymnosperm burning at Lake Victoria (low values of <0.2, with most <0.1), the highest value in the record (0.18) does occur at ~4.1 ka. It is plausible that the charcoal records are more sensitive to distal conifer burning that is not captured well in the overall PAHs fluxes. It would follow that the post-AHP charcoal peak represents increased conifer burning, while PAHs indicate savanna/tropical forest burning may have remained low even as rainfall decreased during the termination of the AHP. Pollen data from the site shows that tropical forest vegetation (i.e., Moraceae, Urticaceae) increased during the AHP at the expense of grasses (Fig. 9d) (Kendall, 1969; Temoltzin-Loranca et al., 2023), as large parts of the Victoria basin likely transitioned from a high-fire savanna state to a low-fire forest state. This vegetation shift potentially explains why PAHs indicate fire activity did not increase again at the end of the AHP: the basin had experienced a transition from one stable state (savanna) to another (forest), displaying hysteresis despite the reversal of the increased rainfall event.

Finally, Lake Bosumtwe (Fig. 2, Site #7) currently receives 1390 ± 29 mm yr^{-1} of rainfall, and based on pollen-estimates, rainfall increased to ~1600–1900 mm yr^{-1} during the AHP (Peyron et al., 2006; Shanahan et al., 2015, 2016). Of all the sites examined here, we predict that Bosumtwe should be most likely to show decreased fire activity due to increasing fuel moisture across the AHP and to experience a shift in vegetation states from savanna to predominately humid forest (Fig. 1d). And indeed, both charcoal and levoglucosan records at Lake Bosumtwe indicate fire activity abruptly decreased at the initiation of the AHP (Fig. 9h) (Shanahan et al., 2016). The exclusion of fire was not reversed at the end of the AHP, suggesting a transition in alternative stable state occurred

(Fig. 1d). Within ~300 years of the decrease in fire and increase in rainfall, leaf wax carbon isotope records indicate vegetation shifted abruptly from C_4 to C_3 dominated plant communities, which was interpreted as a transition from savanna to forest ecosystems (Fig. 9g–i) (Shanahan et al., 2016). Thus, fire and vegetation dynamics at Bosumtwe also conform to expectations.

5.4. Fire response to the African Humid Period across the savanna rainfall gradient

In sum, responses of fire activity at seven paleoecological sites strongly demonstrate that hydroclimatic controls on savanna fire activity vary along a rainfall gradient across African savannas, and that fire responses to climate perturbation depend on initial vegetation and rainfall at a site (Fig. 10). The empirical observations (Fig. 10) closely matched predictions based on our modern understanding fire responses to rainfall (Fig. 1). Arid sites (Site #1: GeoB7920-2, and Site #2: Turkana) showed evidence that prior to the onset of increased AHP precipitation, fuel-loads limited fire activity. Fire activity increased as AHP rainfall increased (Fig. 10). At semi-arid GeoB9508-5 (Site #3), fire controls transitioned from fuel-load limited to fuel-moisture limited, evidenced by first an increase followed by a decrease in fire activity in response to increased AHP rainfall (Fig. 10). Fuel dynamics differed slightly at semi-arid Chala (Site #4, where rainfall increases are likely smaller than other sites). Chala fire activity only marginally increased during the AHP, likely in response to slight increases in rainfall.

Meanwhile, semi-mesic/mesic sites (Site #5: Tanganyika, Site #6: Victoria, Site #7: Bosumtwe) showed evidence of fuel-moisture limited fire regimes, fire activity decreased in as rainfall increased during the AHP (Fig. 9; Fig 10). Tanganyika may have started out as fuel-load limited, transitioning to fuel-moisture limitation after the Younger Dryas, but Victoria and Bosumtwe showed decreased fire activity with the onset of the AHP, suggesting they were already in a primarily fuel-moisture limited regime.

Dynamics across all of these sites may in part reflect decreases in seasonality across the AHP, not just increases in overall MAP. Both isotopic modeling work and $\delta^{18}O$ of herbivore tooth enamel suggest increases in dry season P-E may be especially responsible for the hydroclimate signal observed during the AHP in East Africa (Reid et al., 2019; Tierney et al., 2011a). In fuel-moisture limited systems (all three mesic sites), shorter dry seasons reduce fuel curing and thus reduce fire spread (from modern systems Archibald et al., 2009; Mondal and Sukumar, 2016), compounding increases in MAP to favor forests at the expense of savannas (Aleman et al., 2020; Staver et al., 2011b). Overall, fire records at sites examined here support the interpretation that the AHP partially resulted from increased precipitation during the dry season and/or “short rains” in East Africa.

Together, differential AHP fire behavior across a rainfall gradient reveals that fire-rainfall relationships are non-linear, even on millennial time scales. Recent analysis of Quaternary paleofire activity across a latitudinal gradient in northern Africa supported the intermediate fire hypothesis (Moore et al., 2022): that savanna fire activity is highest at intermediate rainfall (Archibald and Hempson, 2016; Krawchuk and Moritz, 2011). Our analysis, which included some of these same North African sites, corroborates these conclusions across both eastern and western Africa (Fig. 10), and clearly indicates that it is not just the amount of fire activity which shifts as rainfall increases along this gradient, but the direction of the relationship between rainfall and fire (Fig. 10) (Alvarado et al., 2020). Additionally, we found evidence that fire activity responses to rainfall can be reversible (e.g., Site #2: Turkana) or irreversible (e.g., Site #7: Bosumtwe) depending on whether vegetation shifted alongside fire activity.

All three semi-mesic/mesic sites experienced complete declines in fire activity which were not reversed at the end of the AHP and were accompanied by transitions from grass-dominated savannas to *miombo* dry or humid forests (Fig. 9) (Fig. 1c). This suggests that these mesic sites experienced a rainfall-driven state change, which was maintained via hysteresis even after rainfall decreased again to its pre-AHP levels. At the two wettest sites, savanna transitioned to tropical forest via dynamics widely hypothesized from modern savanna-forest bistability. Once a site is forested, moist-closed canopy taxa can inhibit fire—a stabilizing forest feedback at a rainfall range (700–1900 mm yr^{-1}) where regular burning could otherwise maintain savanna (Pausas and Bond, 2020; Staver et al., 2011a).

However, these transitions are not truly irreversible. If ignitions increase enough, we predict the system could shift across the threshold in the opposite direction. At ~2 ka, well after then end of the AHP, forests collapsed at many sites across East Africa, including Lake Victoria (Fig. 11a) (Kendall, 1969), Lake Edward (Ivory and Russell, 2018) and Lake Albert (Beuning et al., 1997). To examine if fire played a role in late Holocene forest-savanna transitions at Lake Victoria, we combine our new PAH record with that of Battistel et al. (2017), who measured PAH concentrations in the same core from late Holocene samples (2.1–1.2 ka). Though Battistel et al. (2017) did not correct for pyrogenic inputs and measured a slightly different suite of compounds, the concentrations of an uncorrected subset of PAHs (3,4, and 5-ring compounds) are comparable between studies (Fig. 11a). The combined record indicates there was no substantial shift in fire or forest-savanna state as rainfall decreased during termination of the AHP, but that at 2.5 ka, fire and grasses increased substantially as woody components decreased (Fig. 11a). Previous work attributed regional forest collapse to a marked increases in fire, driven by a combination of a severe transient drought and increased human ignitions (Battistel et al., 2017; Ivory and Russell, 2018) (Fig. 11b). This is consistent with observations at Victoria, and together indicates while there is hysteresis in these systems, a large enough increase in fire activity can trigger a vegetation state change from forest back to savanna.

Interestingly, Lake Tanganyika also appeared to undergo a state change from savanna to forest in the late Pleistocene that was not reversed during the termination of the AHP or after. Curiously, in addition to an increase in forest taxa during the AHP (Fig. 9a), there is also a shift in composition from tropical forest to a dry forest, largely composed of *miombo* taxa (Fig. 9a). The shift was associated with a strong but not complete reduction in fire activity (Fig. 9a). Today, the *miombo* is a highly flammable ecosystem that functions over large parts of its range as a savanna (Frost, 1996; Ryan and Williams, 2011). However, at least some parts of the *miombo* are considered to be a fire-sensitive forest (Cauldwell and Zieger, 2000; Ryan and Williams, 2011), which appears more consistent with the strong decrease in fire activity that accompanied *miombo* colonization during the AHP. Pollen assemblages indicate that the *miombo* component during the AHP was composed of mostly humid *miombo* taxa, such as *Uapaca* (Ivory and Russell, 2016), a fire-sensitive broad-leaf tree that can reduce understory fuels and fire frequency (Hollingsworth et al., 2015). It is also noteworthy that, in this case, this dry forest system appears to be alternatively stable to more flammable savannas (since it did not revert to its original fire-prone state even after the AHP terminated), a dynamic not usually proposed by those that consider *miombo* a dry forest (Ribeiro et al., 2020).

5.5. Additional factors that may influence savanna fire activity

Other potential influences of fire activity exist besides rainfall and rainfall seasonality. Feedbacks between fire, fuels, savanna, and

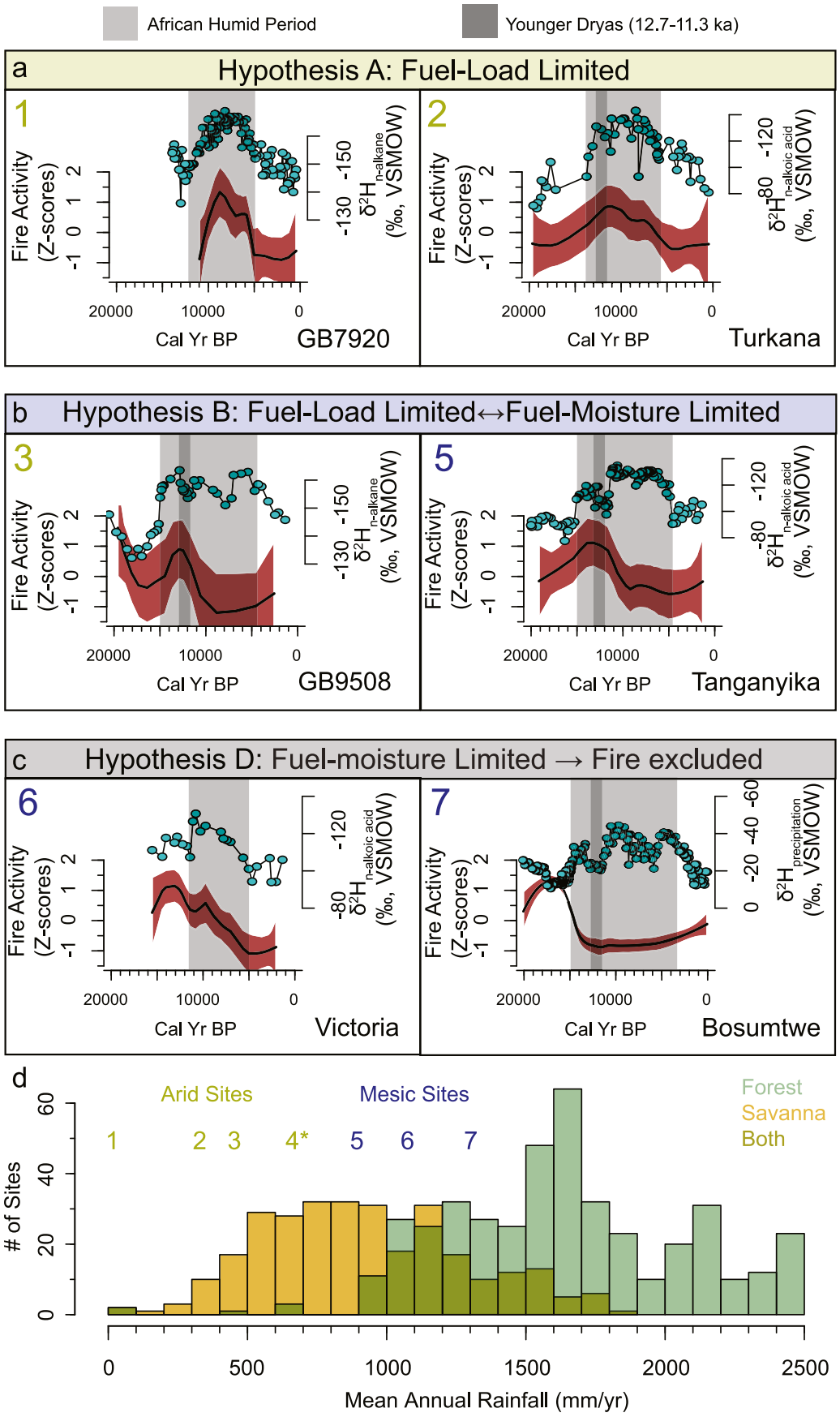
African Humid Period
Younger Dryas (12.7-11.3 ka)
a
Hypothesis A: Fuel-Load Limited
1
2
Fire Activity (Z-scores)
-1 0 1 2
20000 10000 0
Cal Yr BP
GB7920
Turkana
-130 -150
-80 -120
δ²H n-alkane (‰, VSMOW)
δ²H n-alkoic acid (‰, VSMOW)
b
Hypothesis B: Fuel-Load Limited↔Fuel-Moisture Limited
3
5
GB9508
Tanganyika
c
Hypothesis D: Fuel-moisture Limited → Fire excluded
6
7
Victoria
Bosumtwe
0 -20 -40 -60
δ²H precipitation (‰, VSMOW)
d
Arid Sites
Mesic Sites
1 2 3 4* 5 6 7
Forest
Savanna
Both
# of Sites
0 20 40 60
0 500 1000 1500 2000 2500
Mean Annual Rainfall (mm/yr)

forest states are also moderated by abiotic (e.g., pCO_2) and biotic (e.g., herbivory) factors, in addition to hydroclimate, that can confound fire-vegetation-hydroclimate relationships.

Firstly, pCO_2 potentially affects plant physiological function, with differential effects across different plant types that govern the fire and vegetation dynamics discussed here. Savanna grasses generally use the C_4 pathway, which confers an advantage both under low pCO_2 and under water stress (Ehleringer et al., 1997), whereas savanna and forest trees use the C_3 pathway, which is favored under high pCO_2 and/or under humid conditions. Though, pCO_2 shifts have a more direct effect on the balance between C_3 versus C_4 grasses (rather than C_4 grasses versus C_3 trees), pCO_2 may interact with other factors (e.g., moisture balance, fire) to differentiate between trees and grasses (Bond, 2008). Today, increased pCO_2 levels have been linked to increases in the savanna woody fraction (Bond, 2008; Hoffmann et al., 2000). In the past, global pCO_2 levels increased by about 60 ppm from 17–12 ka during the last deglaciation (Monnin et al., 2001), and as moisture increased and fire decreased at fuel-moisture limited sites during the AHP, this increased pCO_2 may have additionally stabilized C_3 trees. This mechanism has been specifically invoked for the state transitions observed at Lake Bosumtwe (Shanahan et al., 2016), as well as to explain shifts in late Holocene savanna and forest climate envelopes across Africa (Phelps et al., 2020). It may also help explain why Tanganyika not only transitioned from fuel-load to fuel-moisture limited, but also to woodier Miombo from more open savanna. This higher pCO_2 may also be implicated in stabilizing forests even at lower precipitation after the termination of AHP (Brovkin et al., 1998).

Second, herbivory may also impact savanna fire activity (Karp et al., 2021b). Grazers reduce grassy fuel loads in savanna systems (Staver et al., 2021; Staver and Bond, 2014), which can reduce fire frequency and burned area (Waldram et al., 2008). As such, herbivore effects on vegetation could have mediated fire responses to rainfall changes over the AHP. However, the size and direction of these effects is not necessarily straightforward. In savannas, herbivore diversity and densities vary along the savanna rainfall gradient (Hempson et al., 2015; Olff et al., 2002), with highest herbivore densities falling between 600 and 800 mm yr^{-1}. It is very likely that Holocene herbivore densities would have also responded to shifting rainfall during the AHP, but like fire, this response may have varied along the rainfall gradient. Of the sites examined here only two, Chala and Tanganyika, capture herbivore patterns via the *Sporormiella* proxy, a fungus that grows on herbivore dung (Ivory and Russell, 2016; Perrotti and van Asperen, 2019; van Geel et al., 2011). At Chala, *Sporormiella* patterns do not change substantially over the Holocene (van Geel et al., 2011), but at Tanganyika, *Sporormiella* values are highest during the AHP, which suggests increased herbivore densities may have stabilized *miombo* and savanna landscapes, as well as helped to exclude fire (Ivory and Russell, 2016). Given the disparate fire dynamics across sites, more work is needed to explicitly tease apart the relative size of the effects of herbivory versus the effects of rainfall on fuel loads during the AHP.

A final factor that may impact savanna fire activity is human activities. In savannas, humans alter fire activity by shifting the timing of fires or by decreasing fuel loads through land use change

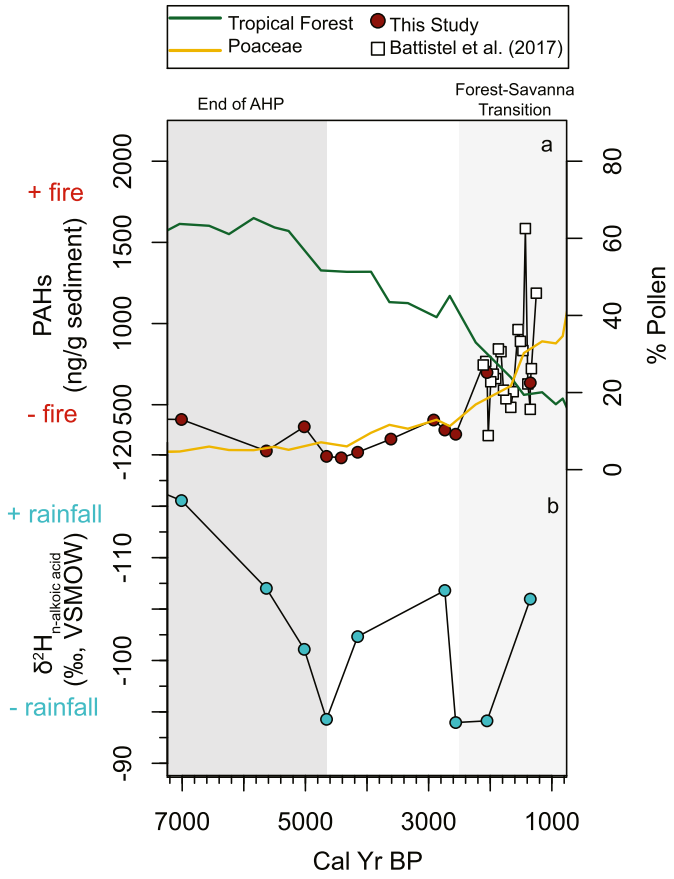

Fig. 11. Post-AHP dynamics at Lake Victoria. The dark grey bar indicates the termination of the AHP, and the light grey bar indicates the transition (~2.5 ka) back from forest to Savanna. a) Left axis is PAH concentrations for the sum of 3,4,5-ring PAHs (Phen, Ant, Fla, Pyr, Chry, BaA). Red circles are from this study. White squares are from Battistel et al. (2017). Right axis is pollen type percentages at Lake Victoria (Kendall, 1969). Tropical Forest = Moraceae, Urticaceae, *Trema*, *Macaranga*, and *Celtis*. b) Leaf wax δ^2H (C_{28} *n*-alkanoic acid) at Lake Victoria (Berke et al., 2012).

(Archibald et al., 2012; Mcwethy et al., 2013). While it is challenging to unambiguously test if humans influenced paleofire activity, we propose some reasonable expectations for how human activities may have altered fire across the rainfall gradient examined here (Mcwethy et al., 2013). At the arid end of the rainfall gradient, in fuel-load limited savannas, human activity could have reduced fire activity by reducing fuel connectivity through either increased grazing or planting (Krawchuk and Moritz, 2011; Mcwethy et al., 2013). At the mesic end of the rainfall gradient, in fuel-moisture limited savannas, human activity could have increased fire activity by increasing dry-season ignitions (Krawchuk and Moritz, 2011; Mcwethy et al., 2013). In both cases, these effects are opposite to how we hypothesized fire would respond to rainfall changes during the AHP. Since our data supports predictions based on rainfall controls (Fig. 10), human drivers were likely not the dominant factor influencing the large-scale fire patterns observed during the AHP. A minimal role for humans in shaping fire regimes during the AHP is also consistent in timing for human technological

Fig. 10. Fire response to the AHP across the modern savanna rainfall gradient a-c) Plots of leaf wax δ^2H records in teal and fire activity Z-scores in maroon from AHP sites. Fire activity is smoothed with 'loess' using a 0.5 span. The shaded region is the 97.5% confidence interval. a) Corresponds to Hypothesis A in Fig. 1 and) GeoB7920 (Dupont and Schefuß, 2018) 2) Lake Turkana (Morrissey, 2014) b) Corresponds to Hypothesis B in Figs. 1 and 3) GeoB9508 (Niedermeyer et al., 2010; Moore et al., 2022) 4) Lake Chala not shown in panel because P-E does not increase at this site during the AHP, but #4 in (b) is where Chala sits relative to the other sites 5) Lake Tanganyika (Ivory and Russell, 2016; Tierney et al., 2008) c) Corresponds to Hypothesis D in Fig. 1 6) Lake Victoria (Berke et al., 2012) 7) Lake Bosumtwe (Shanahan et al., 2015, 2016). b) Modern savanna and forest distribution gradient defined using data from modern Africa floral survey sites replotted from Aleman et al. (2020). Numbers correspond to sites in (a–c). Blue numbers are sites on the mesic side of the rainfall gradient, and yellow numbers are sites on the arid side of the rainfall gradient.

development in this region. Agropastoralism, which had a marked impact on fire activity (Davies et al., 2022), did not expand in West and East Africa until <4 ka, after the termination of the AHP (Archibald et al., 2012; Smith, 1992). And as discussed above, at 2 ka, human activity certainly had a substantial impact on fire activity and shifting forest-savanna states at some of the sites examined here (Ivory and Russell, 2018). These past human-fire dynamics, along with the observation that humans are suppressing fire activity across Africa today (Andela et al., 2017), indicate anthropogenic effects should be taken into account alongside climate variables when making predictions about fire responses to future shifts in rainfall.

6. Conclusions

We set out to test if savanna fire response to the AHP was predictable based on fuel-load and fuel-moisture controls on fire. In modern savannas, spatial patterns indicate fuel controls on fire vary across a rainfall gradient, and that sites may cross fire-fuel thresholds as rainfall increases (Alvarado et al., 2020). During the AHP, we hypothesized savanna fire activity would respond differently to widespread rainfall increases depending on the initial rainfall conditions at a site: that fire activity would increase at fuel-load limited semi-arid sites but decrease at fuel-moisture limited mesic sites. We found that fire response to the AHP varied and was predictable based on our hypothesis. At the most arid sites, fire activity increased during the AHP (GeoB7920 and Lake Turkana) (Fig. 10a; b). At two intermediate sites, fire activity first increased then decreased, indicating transitions from fuel-load limited systems and fuel-moisture limited systems (GeoB9508 and Lake Tanganyika) (Fig. 10c; d). And at the most mesic sites, fire activity decreased during the AHP (Lakes Victoria, and Bosumtwe) (Fig. 10e; f). In modern savannas, spatial patterns also indicate fire stabilizes the vegetation at intermediate rainfall (1000–2000 mm yr^{-1}) and savannas can transition to forest when fire is limited (Aleman and Staver, 2018; Staver et al., 2011a, 2011b). During the AHP, we also hypothesized that if fire was suppressed as rainfall increases at mesic sites, that the sites would transition from savanna to forest. We found evidence for fire-mediated forest transitions during the AHP at all three of our most mesic sites (Lakes Tanganyika, Victoria, and Bosumtwe).

Fire and vegetation responses to decreasing rainfall at the end of the AHP also varied predictably across sites. At the fuel-load limited sites, fire activity decreased as rainfall decreased (GeoB7920 and Lake Turkana). However, at mesic sites that transitioned to forest (Lakes Tanganyika, Victoria, and Bosumtwe), fire did not increase again, even though rainfall decreased to match pre-AHP levels, and forest remained dominant at all three sites. This pattern indicates hysteresis and provides evidence for forest-savanna bistability: once a site is forested, the forest microenvironment inhibits fire, which prevents a transition back to savanna in response to decreasing rainfall. However, it is likely that if fire activity increases enough, sites can shift back across the savanna-forest threshold; for instance, at 2 ka, well after the AHP, human activities combined with drought increased fire activity at some mesic forest sites (e.g., Lake Victoria, Lake Edward), transitioning them back to savanna.

Taken together, variation in fire response across sites indicates that rainfall is a primary control on biomass burning in African savannas and understanding the initial hydroclimate conditions at a particular site is critical for predicting fire response to long-term shifts in rainfall though time. This synthesis of fire across the AHP supports the need for new broad-scale analyses of paleofire activity alongside past hydroclimatic change, which will be a useful tool for benchmarking global fire models (Braconnot et al., 2012; Van Marle et al., 2017).

Author contributions statement

Allison T. Karp: Conceptualization, Methodology, Validation, Formal analysis, Investigation, Writing-Original Draft, Writing-Review, Visualization, Project administration, Funding acquisition; **Kevin T. Uno:** Methodology, Resources, Supervision, Writing-Review; **Melissa A. Berke:** Resources, Investigation, Writing-Review; **James M. Russell:** Resources, Writing-Review, Supervision; **Christopher A. Scholz:** Resources, Writing-Review; **Jennifer R. Marlon:** Writing-Review; **J. Tyler Faith:** Conceptualization, Funding acquisition, Writing-Review; **A. Carla Staver:** Conceptualization, Supervision, Project administration, Funding acquisition, Writing-Review.

Declaration of competing interest

The authors declare that they have no known competing financial interests or personal relationships that could have appeared to influence the work reported in this paper.

Data availability

Data is avalible in the NOAA WDS Paleoclimate Database at: https://www.ncei.noaa.gov/access/paleo-search/study/37384.

Acknowledgements

ATK and ACS were supported by the National Science Foundation [NSF-MSB #1802453], and ATK was supported by the National Science Foundation [NSF-EAR #2204471]. Collaboration between ATK, ACS, and JTF was supported the National Science Foundation [NSF-DEB #2224317/2224318]. JMR was supported by the National Science Foundation [NSF-DEB-2048669], KTU was supported by the Vetlesen Foundation and Center for Climate and Life Fellowship from Columbia University.

Appendix A. Supplementary data

Supplementary data to this article can be found online at https://doi.org/10.1016/j.quascirev.2023.107994.

References

Adie, H., Lawes, M.J., 2011. Podocarps in africa: temperate zone relicts or rainforest survivors? Smithsonian Contrib. Bot. 79–100. https://doi.org/10.5479/si.0081024x.95.79.

Aleman, J.C., Staver, A.C., 2018. Spatial patterns in the global distributions of savanna and forest. Global Ecol. Biogeogr. 27, 792–803. https://doi.org/10.1111/geb.12739.

Aleman, J.C., Fayolle, A., Favier, C., Staver, A.C., Dexter, K.G., Ryan, C.M., Azihou, A.F., Bauman, D., te Beest, M., Chidumayo, E.N., Comiskey, J.A., Cromsigt, J.P.G.M., Dessard, H., Doucet, J.L., Finckh, M., Gillet, J.F., Gourlet-Fleury, S., Hempson, G.P., Holdo, R.M., Kirunda, B., Kouame, F.N., Mahy, G., Maiato, F., Gonçalves, P., McNicol, I., Nieto Quintano, P., Plumptre, A.J., Pritchard, R.C., Revermann, R., Schmitt, C.B., Swemmer, A.M., Talila, H., Woollen, E., Swaine, M.D., 2020. Floristic evidence for alternative biome states in tropical Africa. Proc. Natl. Acad. Sci. U.S.A. 117, 28183–28190. https://doi.org/10.1073/pnas.2011515117.

Alvarado, S.T., Andela, N., Silva, T.S.F., Archibald, S., 2020. Thresholds of fire response to moisture and fuel load differ between tropical savannas and grasslands across continents. Global Ecol. Biogeogr. 29, 331–344. https://doi.org/10.1111/geb.13034.

Andela, N., Morton, D.C., Giglio, L., Chen, Y., Van Der Werf, G.R., Kasibhatla, P.S., DeFries, R.S., Collatz, G.J., Hantson, S., Kloster, S., Bachelet, D., Forrest, M., Lasslop, G., Li, F., Mangeon, S., Melton, J.R., Yue, C., Randerson, J.T., 2017. A human-driven decline in global burned area. Science 84 356, 1356–1362. https://doi.org/10.1126/science.aal4108.

Aragão, L.E.O.C., Malhi, Y., Barbier, N., Lima, A., Shimabukuro, Y., Anderson, L., Saatchi, S., 2008. Interactions between rainfall, deforestation and fires during recent years in the Brazilian Amazonia. Philos. Trans. R. Soc. B Biol. Sci. 363, 1779–1785. https://doi.org/10.1098/rstb.2007.0026.

Archibald, S., Hempson, G.P., 2016. Competing consumers: contrasting the patterns

and impacts of fire and mammalian herbivory in Africa. Philos. Trans. R. Soc. B Biol. Sci. 371. https://doi.org/10.1098/rstb.2015.0309.
Archibald, S., Roy, D.P., van Wilgen, B.W., Scholes, R.J., 2009. What limits fire? An examination of drivers of burnt area in Southern Africa. Global Change Biol. 15, 613–630. https://doi.org/10.1111/j.1365-2486.2008.01754.x.
Archibald, S., Staver, A.C., Levin, S.A., 2012. Evolution of human-driven fire regimes in Africa. Proc. Natl. Acad. Sci. U.S.A. 109, 847–852. https://doi.org/10.1073/pnas.1118648109.
Barker, P.A., Hurrell, E.R., Leng, M.J., Wolff, C., Cocquyt, C., Sloane, H.J., Verschuren, D., 2011. Seasonality in equatorial climate over the past 25 k.y. Revealed by oxygen isotope records from Kilimanjaro. Geology 39, 1111–1114. https://doi.org/10.1130/G32419.1.
Battistel, D., Argiriadis, E., Kehrwald, N., Spigariol, M., Russell, J.M., Barbante, C., 2017. Fire and human record at Lake Victoria, East Africa, during the early iron age: did humans or climate cause massive ecosystem changes? Holocene 27, 997–1007.
Bergner, A.G.N., Trauth, M.H., Bookhagen, B., 2003. Paleoprecipitation estimates for the Lake Naivasha basin (Kenya) during the last 175 k.y. using a lake-balance model. Global Planet. Change 36, 117–136. https://doi.org/10.1016/S0921-8181(02)00178-9.
Berke, M.A., Johnson, T.C., Werne, J.P., Grice, K., Schouten, S., Sinninghe Damsté, J.S., 2012. Molecular records of climate variability and vegetation response since the late Pleistocene in the Lake Victoria basin, East Africa. Quat. Sci. Rev. 55, 59–74. https://doi.org/10.1016/j.quascirev.2012.08.014.
Berke, M.A., Johnson, T.C., Werne, J.P., Livingstone, D.A., Grice, K., Schouten, S., Sinninghe Damsté, J.S., 2014. Characterization of the last deglacial transition in tropical East Africa: insights from Lake Albert. Palaeogeogr. Palaeoclimatol. Palaeoecol. 409, 1–8. https://doi.org/10.1016/j.palaeo.2014.04.014.
Beuning, K.R.M., Russell, J.M., 2004. Vegetation and sedimentation in the Lake Edward basin, Uganda–Congo during the late Pleistocene and early Holocene. J. Paleolimnol. 32, 1–18.
Beuning, K.R.M., Talbot, M.R., Kelts, K., 1997. A revised 30,000-year paleoclimatic and paleohydrologic history of Lake Albert, East Africa. Palaeogeogr. Palaeoclimatol. Palaeoecol. 136, 259–279. https://doi.org/10.1016/S0031-0182(97)00034-5.
Blaauw, M., Christeny, J.A., 2011. Flexible paleoclimate age-depth models using an autoregressive gamma process. Bayesian Anal 6, 457–474. https://doi.org/10.1214/11-BA618.
Blaauw, M., van Geel, B., Kristen, I., Plessen, B., Lyaruu, A., Engstrom, D.R., van der Plicht, J., Verschuren, D., 2011. High-resolution 14C dating of a 25,000-year lake-sediment record from equatorial East Africa. Quat. Sci. Rev. 30, 3043–3059. https://doi.org/10.1016/j.quascirev.2011.07.014.
Blumer, M., Youngblood, W.W., 1975. Polycyclic aromatic hydrocarbons in soils and recent sediments. Science 84 188, 53–55.
Bond, W.J., 2008. What limits trees in C 4 grasslands and savannas? Annu. Rev. Ecol. Evol. Syst. 39, 641–659. https://doi.org/10.1146/annurev.ecolsys.39.110707.173411.
Bonnefille, R., Chalie, F., 2000. Pollen-inferred precipitation time-series from equatorial mountains, Africa, the last 40 kyr BP. Global Planet. Change 26, 25–50. https://doi.org/10.1016/S0921-8181(00)00032-1.
Braconnot, P., Harrison, S.P., Kageyama, M., Bartlein, P.J., Masson-Delmotte, V., Abe-Ouchi, A., Otto-Bliesner, B., Zhao, Y., 2012. Evaluation of climate models using palaeoclimatic data. Nat. Clim. Change 2, 417–424. https://doi.org/10.1038/nclimate1456.
Brovkin, V., Claussen, M., Petoukhov, V., 1998. On the stability of the atmosphere-vegetation system in the Sahara/Sahel region. J. Geophys. Res. 103.
Buckles, L.K., Weijers, J.W.H., Verschuren, D., Sinninghe Damsté, J.S., 2014. Sources of core and intact branched tetraether membrane lipids in the lacustrine environment: anatomy of Lake Challa and its catchment, equatorial East Africa. Geochem. Cosmochim. Acta 140, 106–126. https://doi.org/10.1016/j.gca.2014.04.042.
Cauldwell, A.E., Zieger, U., 2000. A reassessment of the fire-tolerance of some miombo woody species in the Central Province, Zambia. Afr. J. Ecol. 38, 138–146>. https://doi.org/10.1046/j.1365-2028.2000.00232.x.
Cockerton, H.E., Street-Perrott, F.A., Barker, P.A., Leng, M.J., Sloane, H.J., Ficken, K.J., 2015. Orbital forcing of glacial/interglacial variations in chemical weathering and silicon cycling within the upper White Nile basin, East Africa: stable-isotope and biomarker evidence from Lakes Victoria and Edward. Quat. Sci. Rev. 130, 57–71. https://doi.org/10.1016/j.quascirev.2015.07.028.
Collins, J.A., Schefuß, E., Mulitza, S., Prange, M., Werner, M., Tharammal, T., Paul, A., Wefer, G., 2013. Estimating the hydrogen isotopic composition of past precipitation using leaf-waxes from western Africa. Quat. Sci. Rev. 65, 88–101. https://doi.org/10.1016/j.quascirev.2013.01.007.
Colombaroli, D., Ssemmada, I., Gelorini, V., Verschuren, D., 2014. Contrasting long-term records of biomass burning in wet and dry savannas of equatorial East Africa. Global Change Biol.
Core, T.R., 2019. R: A Language and Environment for Statistical Computing.
Daniau, A.L., Bartlein, P.J., Harrison, S.P., Prentice, I.C., Brewer, S., Friedlingstein, P., Harrison-Prentice, T.I., Inoue, J., Izumi, K., Marlon, J.R., Mooney, S., Power, M.J., Stevenson, J., Tinner, W., Andrič, M., Atanassova, J., Behling, H., Black, M., Blarquez, O., Brown, K.J., Carcaillet, C., Colhoun, E.A., Colombaroli, D., Davis, B.A.S., D'Costa, D., Dodson, J., Dupont, L., Eshetu, Z., Gavin, D.G., Genries, A., Haberle, S., Hallett, D.J., Hope, G., Horn, S.P., Kassa, T.G., Katamura, F., Kennedy, L.M., Kershaw, P., Krivonogov, S., Long, C., Magri, D., Marinova, E., McKenzie, G.M., Moreno, P.I., Moss, P., Neumann, F.H., Norstrm, E., Paitre, C., Rius, D., Roberts, N., Robinson, G.S., Sasaki, N., Scott, L., Takahara, H., Terwilliger, V., Thevenon, F., Turner, R., Valsecchi, V.G., Vannière, B., Walsh, M., Williams, N., Zhang, Y., 2012. Predictability of biomass burning in response to climate changes. Global Biogeochem. Cycles 26, 1–12. https://doi.org/10.1029/2011GB004249.
Dansgaard, W., 1964. Stable isotopes in precipitation. Tellus 16, 436–468. https://doi.org/10.3402/tellusa.v16i4.8993.
Davies, B., Power, M.J., Braun, D.R., Douglass, M.J., Mosher, S.G., Quick, L.J., Esteban, I., Sealy, J., Parkington, J., Faith, J.T., 2022. Fire and human management of late Holocene ecosystems in southern Africa. Quat. Sci. Rev. 289, 107600. https://doi.org/10.1016/j.quascirev.2022.107600 deMenocal.
deMenocal, P.B., Ortiz, J., Guilderson, T., Adkins, J., Sarnthein, M., Baker, L., Yarusinsky, M., 2000. Abrupt onset and termination of the African Humid Period: rapid climate responses to gradual insolation forcing. Quat. Sci. Rev. 19, 347–361.
Denis, E.H., Pedentchouk, N., Schouten, S., Pagani, M., Freeman, K.H., 2017. Fire and ecosystem change in the arctic across the paleocene–eocene thermal maximum. Earth Planet Sci. Lett. 467, 149–156. https://doi.org/10.1016/j.epsl.2017.03.021.
Dunning, C.M., Black, E., Allan, R.P., 2018. Later wet seasons with more intense rainfall over Africa under future climate change. J. Clim. 31, 9719–9738. https://doi.org/10.1175/JCLI-D-18-0102.1.
Dupont, L.M., Schefuß, E., 2018. The roles of fire in Holocene ecosystem changes of West Africa. Earth Planet Sci. Lett. 481, 255–263. https://doi.org/10.1016/j.epsl.2017.10.049.
Ebisuzaki, W., 1997. A method to estimate the statistical significance of a correlation when the data are serially correlated. J. Clim. 10, 2147–2153.
Ehleringer, J.R., Cerling, T.E., Helliker, B.R., 1997. C4 photosynthesis, atmospheric CO2, and climate. Oecologia 112, 285–299. https://doi.org/10.3760/cma.-j.issn.0254-6450.2011.05.005.
Fick, S.E., Hijmans, R.J., 2017. WorldClim 2: new 1km spatial resolution climate surfaces for global land areas. Int. J. Climatol. 37, 4302–4312.
Fischer, M.L., Markowska, M., Bachofer, F., Foerster, V.E., Asrat, A., Zielhofer, C., Trauth, M.H., Junginger, A., 2020. Determining the pace and magnitude of Lake level changes in southern Ethiopia over the last 20,000 Years using lake balance modeling and SEBAL. Front. Earth Sci. 8, 1–21. https://doi.org/10.3389/feart.2020.00197.
Frost, P., 1996. The ecology of miombo woodlands. In: Campbell, B. (Ed.), The Miombo in Transition: Woodlands and Welfare in Africa. Centre for International Forestry Research, Bogor, Indonesia, p. 266.
Garcin, Y., Melnick, D., Strecker, M.R., Olago, D., Tiercelin, J.J., 2012. East African mid-Holocene wet-dry transition recorded in palaeo-shorelines of Lake Turkana, northern Kenya Rift. Earth Planet Sci. Lett. 331 (332), 322–334. https://doi.org/10.1016/j.epsl.2012.03.016.
Gaujoux, R., Seoighe, C., 2010. A flexible R package for nonnegative matrix factorization. BMC Bioinf. 2010, 11.
Giglio, L., van der Werf, G.R., Randerson, J.T., Collatz, G.J., Kasibhatla, P., 2006. Global estimation of burned area using MODIS active fire observations. Atmos. Chem. Phys. 6, 957–974. https://doi.org/10.5194/acp-6-957-2006.
Haile, G.G., Tang, Q., Hosseini-Moghari, S.M., Liu, X., Gebremicael, T.G., Leng, G., Kebede, A., Xu, X., Yun, X., 2020. Projected impacts of climate change on drought patterns over East Africa. Earth's Future 8, 1–23. https://doi.org/10.1029/2020EF001502.
He, T., Lamont, B.B., 2017. Baptism by fire: the pivotal role of ancient conflagrations in evolution of the Earth's flora. Natl. Sci. Rev. 1–18. https://doi.org/10.1093/nsr/nwx041.
Hempson, G.P., Archibald, S., Bond, W.J., 2015. A continent-wide assessment of the form and intensity of large mammal herbivory in Africa. Science 350 (80), 1056–1061. https://doi.org/10.1126/science.aac7978.
Hoffmann, W.A., Bazzaz, F.A., Chatterton, N.J., Harrison, P.A., Jackson, R.B., 2000. Elevated CO2 enhances resprouting of a tropical savanna tree. Oecologia 123, 312–317. https://doi.org/10.1007/s004420051017.
Hoffmann, W.A., Geiger, E.L., Gotsch, S.G., Rossatto, D.R., Silva, L.C.R., Lau, O.L., Haridasan, M., Franco, A.C., 2012. Ecological thresholds at the savanna-forest boundary: how plant traits, resources and fire govern the distribution of tropical biomes. Ecol. Lett. 15, 759–768. https://doi.org/10.1111/j.1461-0248.2012.01789.x.
Hollander, M., Wolfe, D., 1973. Nonparametric Statistical Methods. John Wiley & Sons, New York.
Hollingsworth, L.T., Johnson, D., Sikaundi, S.S., 2015. Fire Management Assessment of Eastern Province, Zambia. Washington, D. C. https://doi.org/10.13140/RG.2.1.1544.2407.
Holmes, J., Hoelzmann, P., 2017. The late pleistocene-holocene African Humid Period as evident in lakes. In: Oxford Research Encyclopedia of Climate Science, pp. 1–41. https://doi.org/10.1093/acrefore/9780190228620.013.531.
Hopmans, E.C., Weijers, J.W.H., Schefuß, E., Herfort, L., Sinninghe Damsté, J.S., Schouten, S., 2004. A novel proxy for terrestrial organic matter in sediments based on branched and isoprenoid tetraether lipids. Earth Planet. Sci. Lett. 224, 107–116. https://doi.org/10.1016/j.epsl.2004.05.012.
Ivory, S.J., Russell, J., 2016. Climate, herbivory, and fire controls on tropical African forest for the last 60ka. Quat. Sci. Rev. 148, 101–114. https://doi.org/10.1016/j.quascirev.2016.07.015.
Ivory, S.J., Russell, J., 2018. Lowland forest collapse and early human impacts at the end of the African Humid Period at Lake Edward, equatorial East Africa. Quat. Res. 89, 7–20. https://doi.org/10.1017/qua.2017.48.

Jenkins, B.M., Jones, A.D., Turn, S.Q., Williams, R.B., 1996. Particle concentrations, gas-particle partitioning, and species intercorrelations for polycyclic aromatic hydrocarbons (PAH) emitted during biomass burning. Atmos. Environ. 30, 3825–3835. https://doi.org/10.1016/1352-2310(96)00084-2.
Johnson, T.C., Kelts, K., Odada, E., 2000. The Holocene history of Lake Victoria. Ambio 29, 2–11. https://doi.org/10.1097/EDE.0b013e3181.
Junginger, A., Trauth, M.H., 2013. Hydrological constraints of paleo-lake suguta in the northern Kenya rift during the African Humid Period (15-5kaBP). Global Planet. Change 111, 174–188. https://doi.org/10.1016/j.gloplacha.2013.09.005.
Kahiu, M.N., Hanan, N.P., 2018. Fire in sub-Saharan Africa: the fuel, cure and connectivity hypothesis. Global Ecol. Biogeogr. 27, 946–957. https://doi.org/10.1111/geb.12753.
Karp, A.T., Behrensmeyer, A.K., Freeman, K.H., 2018. Grassland fire ecology has roots in the late Miocene. Proc. Natl. Acad. Sci. USA 115, 12130–12135. https://doi.org/10.1073/pnas.1809758115.
Karp, A.T., Holman, A.I., Hopper, P., Grice, K., Freeman, K.H., 2020. Fire Distinguishers: refined interpretations of paleofire from polycyclic aromatic hydrocarbons. Geochem. Cosmochim. Acta 289, 93–113. https://doi.org/10.1016/j.gca.2020.08.024.
Karp, A.T., Andrae, J.W., McInerney, F.A., Polissar, P.J., Freeman, K.H., 2021a. Soil carbon loss and weak fire feedbacks during pliocene C_4 grassland expansion in Australia. Geophys. Res. Lett. 48. https://doi.org/10.1029/2020GL090964.
Karp, A.T., Faith, J.T., Marlon, J.R., Staver, A.C., 2021b. Global response of fire activity to late Quaternary grazer extinctions. Science 80.
Karp, A.T., Uno, K.T., Polissar, P.J., Freeman, K.H., 2021c. Late Miocene C 4 grassland fire feedbacks on the Indian Subcontinent. Paleoceanogr. Paleoclimatol. 1–20. https://doi.org/10.1029/2020pa004106.
Kendall, R.L., 1969. An ecological history of the Lake Victoria basin. Ecol. Monogr. 39, 121–176. https://doi.org/10.2307/1950740.
Konecky, B.L., Noone, D.C., Cobb, K.M., 2019. The influence of competing hydroclimate processes on stable isotope ratios in tropical rainfall. Geophys. Res. Lett. 46, 1622–1633. https://doi.org/10.1029/2018GL080188.
Krawchuk, M.A., Moritz, M.A., 2011. Constraints on global fire activity vary across a resource gradient. Ecology 92, 121–132. https://doi.org/10.1890/09-1843.1.
Kutzbach, J.E., Street-Perrott, F.A., 1985. Milankovitch forcing of fluctuations in the level of tropical lakes from 18 to 0 kyr BP. Nature 317, 130–134. https://doi.org/10.1038/317130a0.
Larrasoaña, J.C., Roberts, A.P., Rohling, E.J., 2013. Dynamics of green Sahara periods and their role in hominin evolution. PLoS One 8. https://doi.org/10.1371/journal.pone.0076514.
Lee, D.D., Seung, H.S., 2001. Algorithms for non-negative matrix factorization. Adv. Neural Inf. Process. Syst. 556–562.
Leys, B.A., Commerford, J.L., McLauchlan, K.K., 2017. Reconstructing grassland fire history using sedimentary charcoal: considering count, size and shape. PLoS One. https://doi.org/10.1371/journal.pone.0176445.
Leys, B.A., Marlon, J.R., Umbanhowar, C., Vannière, B., 2018. Global fire history of grassland biomes. Ecol. Evol. 1–22. https://doi.org/10.1002/ece3.4394.
Lima, A.L.C., Farrington, J.W., Reddy, C.M., 2005. Combustion-derived polycyclic aromatic hydrocarbons in the environment—a review. Environ. Forensics 6, 109–131. https://doi.org/10.1080/15275920590952739.
Mallick, S., Chakraborty, J., Dutta, T.K., 2011. Role of oxygenases in guiding diverse metabolic pathways in the bacterial degradation of low-molecular-weight polycyclic aromatic hydrocarbons: a review. Crit. Rev. Microbiol. 37, 64–90. https://doi.org/10.3109/1040841X.2010.512268.
Marlon, J.R., Bartlein, P.J., Carcaillet, C., Gavin, D.G., Harrison, S.P., Higuera, P.E., Joos, F., Power, M.J., Prentice, I.C., 2008. Climate and human influences on global biomass burning over the past two millennia. Nat. Geosci. 1, 697–702. https://doi.org/10.1038/ngeo313.
Marlon, J.R., Kelly, R., Daniau, A.L., Vannière, B., Power, M.J., Bartlein, P., Higuera, P., Blarquez, O., Brewer, S., Brücher, T., Feurdean, A., Romera, G.G., Iglesias, V., Yoshi Maezumi, S., Magi, B., Mustaphi, C.J.C., Zhihai, T., 2016. Reconstructions of biomass burning from sediment-charcoal records to improve data-model comparisons. Biogeosciences 13, 3225–3244. https://doi.org/10.5194/bg-13-3225-2016.
Mcwethy, D.B., Higuera, P.E., Whitlock, C., Veblen, T.T., Bowman, D.M.J.S., Cary, G.J., Haberle, S.G., Keane, R.E., Maxwell, B.D., Mcglone, M.S., Perry, G.L.W., Wilmshurst, J.M., Holz, A., Tepley, A.J., 2013. A conceptual framework for predicting temperate ecosystem sensitivity to human impacts on fire regimes. Global Ecol. Biogeogr. 22, 900–912. https://doi.org/10.1111/geb.12038.
Meyers, S.R., 2014. Astrochron: an R Package for Astrochronology (Cran).
Miller, D.R., Castañeda, I.S., Bradley, R.S., MacDonald, D., 2017. Local and regional wildfire activity in central Maine (USA) during the past 900 years. J. Paleolimnol. 58, 455–466. https://doi.org/10.1007/s10933-017-0002-z.
Mondal, N., Sukumar, R., 2016. Fires in seasonally dry tropical forest: testing the varying constraints hypothesis across a regional rainfall gradient. PLoS One 11, 1–15. https://doi.org/10.1371/journal.pone.0159691.
Monnin, E., Indermühle, A., Dällenbach, A., Flückiger, J., Stauffer, B., Stocker, T.F., Raynaud, D., Barnola, J.M., 2001. Atmospheric CO_2 concentrations over the last glacial termination. Science 291 (80), 112–114. https://doi.org/10.1126/science.291.5501.112.
Moore, M., Kuang, Z., Blossey, P.N., 2014. A moisture budget perspective of the amount effect. Geophys. Res. Lett. 41, 1329–1335. https://doi.org/10.1002/2013GL058302.
Moore, H.R., Crocker, A.J., Belcher, C.M., Meckler, A.N., Osborne, C.P., Beerling, D.J., Wilson, P.A., 2022. Hydroclimate variability was the main control on fire activity in northern Africa over the last 50,000 years. Quat. Sci. Rev. 288, 107578. https://doi.org/10.1016/j.quascirev.2022.107578.
Morrissey, A., 2014. Stratigraphic Framework and Quaternary Paleolimnology of the Lake Turkana Rift, Kenya. PhD Diss. Syracuse University.
Morrissey, A., Scholz, C.A., 2014. Paleohydrology of Lake Turkana and its influence on the nile river system. Palaeogeogr. Palaeoclimatol. Palaeoecol. 403, 88–100. https://doi.org/10.1016/j.palaeo.2014.03.029.
Morrissey, A., Scholz, C.A., Russell, J.M., 2018. Late Quaternary TEX86 paleotemperatures from the world's largest desert lake, Lake Turkana, Kenya. J. Paleolimnol. 59, 103–117. https://doi.org/10.1007/s10933-016-9939-6.
Murphy, B.P., Prior, L.D., Cochrane, M.A., Williamson, G.J., Bowman, D.M.J.S., 2019. Biomass consumption by surface fires across Earth's most fire prone continent. Global Change Biol. 25, 254–268. https://doi.org/10.1111/gcb.14460.
Nelson, D.M., Verschuren, D., Urban, M.A., Hu, F.S., 2012. Long-term variability and rainfall control of savanna fire regimes in equatorial East Africa. Global Change Biol. 18, 3160–3170. https://doi.org/10.1111/j.1365-2486.2012.02766.x.
Niedermeyer, E.M., Schefuß, E., Sessions, A.L., Mulitza, S., Mollenhauer, G., Schulz, M., Wefer, G., 2010. Orbital- and millennial-scale changes in the hydrologic cycle and vegetation in the western African Sahel: insights from individual plant wax δD and δ13C. Quat. Sci. Rev. 29, 2996–3005. https://doi.org/10.1016/j.quascirev.2010.06.039.
Olff, H., Ritchie, M.E., Prins, H.H.T., 2002. Global environmental controls of diversity in large herbivores. Nature 415, 901–904. https://doi.org/10.1038/415901a.
Pausas, J.G., Bond, W.J., 2020. Alternative biome states in terrestrial ecosystems. Trends Plant Sci. 25, 250–263. https://doi.org/10.1016/j.tplants.2019.11.003.
Pearson, K., 1948. Karl Pearson's Early Statistical Papers. University Press, Cambridge, England.
Perrotti, A.G., van Asperen, E., 2019. Dung fungi as a proxy for megaherbivores: opportunities and limitations for archaeological applications. Veg. Hist. Archaeobotany 28, 93–104. https://doi.org/10.1007/s00334-018-0686-7.
Peyron, O., Jolly, D., Braconnot, P., Bonnefille, R., Guiot, J., Wirrmann, D., Chalié, F., 2006. Quantitative reconstructions of annual rainfall in Africa 6000 years ago: model-data comparison. J. Geophys. Res. Atmos. 111, 1–9. https://doi.org/10.1029/2006JD007396.
Phelps, L.N., Chevalier, M., Shanahan, T.M., Aleman, J.C., Courtney-Mustaphi, C., Kiahtipes, C.A., Broennimann, O., Marchant, R., Shekeine, J., Quick, L.J., Davis, B.A.S., Guisan, A., Manning, K., 2020. Asymmetric response of forest and grassy biomes to climate variability across the African Humid Period: influenced by anthropogenic disturbance? Ecography 43, 1118–1142. https://doi.org/10.1111/ecog.04990.
Polissar, P.J., Rose, C., Uno, K.T., Phelps, S.R., deMenocal, P., 2019. Synchronous rise of African C4 ecosystems 10 million years ago in the absence of aridification. Nat. Geosci. 12. https://doi.org/10.1038/s41561-019-0399-2.
Reid, R.E.B., Jones, M., Brandt, S., Bunn, H., Marshall, F., 2019. Oxygen isotope analyses of ungulate tooth enamel confirm low seasonality of rainfall contributed to the African Humid Period in Somalia. Palaeogeogr. Palaeoclimatol. Palaeoecol. 534, 109272. https://doi.org/10.1016/j.palaeo.2019.109272.
Ribeiro, N.S., Miranda, P.L.S. De, Timberlake, J., 2020. Biogeography and ecology of miombo woodlands. In: Miombo Woodlands in a Changing Environment: Securing the Resilience and Sustainability of People and Woodlands. Springer International Publishing, pp. 9–53. https://doi.org/10.1007/978-3-030-50104-4.
Rowell, D.P., Booth, B.B.B., Nicholson, S.E., Good, P., 2015. Reconciling past and future rainfall trends over East Africa. J. Clim. 28, 9768–9788. https://doi.org/10.1175/JCLI-D-15-0140.1.
Rozanski, K., Araguás-Araguás, L., Gonfiantini, R., 1993. Isotopic patterns in modern global precipitation. In: Swart, P.K., Lohmann, K.C., Mckenzie, J., Savin, S. (Eds.), Climate Change in Continental Isotopic Records, pp. 1–36. https://doi.org/10.1029/gm078p0001.
Ryan, C.M., Williams, M., 2011. How does fire intensity and frequency affect miombo woodland tree populations and biomass? Ecol. Appl. 21, 48–60. https://doi.org/10.1890/09-1489.1.
Sachse, D., Billault, I., Bowen, G.J., Chikaraishi, Y., Dawson, T.E., Feakins, S.J., Freeman, K.H., Magill, C.R., McInerney, F.A., van der Meer, M.T.J., Polissar, P., Robins, R.J., Sachs, J.P., Schmidt, H.-L., Sessions, A.L., White, J.W.C., West, J.B., Kahmen, A., 2012. Molecular paleohydrology: interpreting the hydrogen-isotopic composition of lipid biomarkers from photosynthesizing organisms. Annu. Rev. Earth Planet Sci. 40, 221–249. https://doi.org/10.1146/annurev-earth-042711-105535.
Sala, O.E., Gherardi, L.A., Reichmann, L., Jobbágy, E., Peters, D., 2012. Legacies of precipitation fluctuations on primary production: theory and data synthesis. Philos. Trans. R. Soc. B Biol. Sci. 367, 3135–3144. https://doi.org/10.1098/rstb.2011.0347.
Sene, K.J., Plinston, D.T., 1994. A review and update of the hydrology of lake victoria in east africa. Hydrol. Sci. J. 39, 47–63. https://doi.org/10.1080/02626669409492719.
Shanahan, T.M., Overpeck, J.T., Scholz, C.A., Beck, J.W., Peck, J., King, J.W., 2008. Abrupt changes in the water balance of tropical West Africa during the late quaternary. J. Geophys. Res. Atmos. 113, 1–12. https://doi.org/10.1029/2007JD009320.
Shanahan, T.M., Mckay, N.P., Hughen, K.A., Overpeck, J.T., Otto-Bliesner, B., Heil, C.W., King, J., Scholz, C.A., Peck, J., 2015. The time-transgressive termination of the African humid period. Nat. Geosci. 8, 140–144. https://doi.org/10.1038/ngeo2329.
Shanahan, T.M., Hughen, K.A., McKay, N.P., Overpeck, J.T., Scholz, C.A., Gosling, W.D., Miller, C.S., Peck, J.A., King, J.W., Heil, C.W., 2016. CO2 and fire influence tropical

ecosystem stability in response to climate change. Sci. Rep. 6, 29587. https://doi.org/10.1038/srep29587.
Simoneit, 1977. Diterpenoid compounds and other lipids in deep-sea sediments and their geochemical significance. Geochem. Cosmochim. Acta 41, 463–476. https://doi.org/10.1016/0016-7037(77)90285-X.
Simoneit, B.R.T., 1986. Cyclic terpenoids of the geosphere. In: Biological Markers in the Sedimentary Record, pp. 43–99.
Simoneit, B.R.T., 2002. Biomass burning - a review of organic tracers for smoke from incomplete combustion. Appl. Geochem. 17, 129–162. https://doi.org/10.1016/S0883-2927(01)00061-0.
Sinninghe Damsté, J.S., Ossebaar, J., Schouten, S., Verschuren, D., 2012. Distribution of tetraether lipids in the 25-ka sedimentary record of Lake Challa: extracting reliable TEX 86 and MBT/CBT palaeotemperatures from an equatorial African lake. Quat. Sci. Rev. 50, 43–54. https://doi.org/10.1016/j.quascirev.2012.07.001.
Smith, A.B., 1992. Origins and spread of pastoralism in africa. Annu. Rev. Anthropol. 21, 125–141.
Staver, A.C., Bond, W.J., 2014. Is there a "browse trap"? Dynamics of herbivore impacts on trees and grasses in an African savanna. J. Ecol. 102, 595–602. https://doi.org/10.1111/1365-2745.12230.
Staver, A.C., Archibald, S., Levin, S., 2011a. Tree cover in sub-Saharan Africa: rainfall and fire constrain forest and savanna as alternative stable states. Ecology 92, 1063–1072.
Staver, A.C., Archibald, S., Levin, S., 2011b. The global extent and determinants of savanna and forest as alternative biome states. Science 84 334, 230–232. https://doi.org/10.1126/science.1210465.
Staver, A.C., Botha, J., Hedin, L., 2017. Soils and fire jointly determine vegetation structure in an African savanna. New Phytol. 216, 1151–1160. https://doi.org/10.1111/nph.14738.
Staver, A.C., Abraham, J.O., Hempson, G.P., Karp, A.T., Faith, J.T., 2021. The past, present, and future of herbivore impacts on savanna vegetation. J. Ecol.
Stogiannidis, E., Laane, R., 2015. Source characterization of polycyclic aromatic hydrocarbons by using their molecular indices: an overview of possibilities. In: Whitacre, D.M. (Ed.), Reviews of Environmental Contamination and Toxicology. Springer International Publishing, Cham, pp. 49–133. https://doi.org/10.1007/978-3-319-10638-0_2.
Strömberg, C.A.E., Staver, A.C., 2022. The history and challenge of grassy biomes. Science 377, 592–594.
Talbot, M.R., Lærdal, T., 2000. The Late Pleistocene - Holocene palaeolimnology of Lake Victoria, East Africa, based upon elemental and isotopic analyses of sedimentary organic matter. J. Paleolimnol. 23, 141–164. https://doi.org/10.1023/A:1008029400463.
Temoltzin-Loranca, Y., Gobet, E., Vannière, B., van Leeuwen, J.F.N., Wienhues, G., Szidat, S., Courtney-Mustaphi, C., Kishe, M., Muschick, M., Seehausen, O., Grosjean, M., Tinner, W., 2023. A chronologically reliable record of 17,000 years of biomass burning in the Lake Victoria area. Quat. Sci. Rev. 301. https://doi.org/10.1016/j.quascirev.2022.107915.
Tierney, J.E., Russell, J.M., Huang, Y., Sinninghe Damsté, J.S., Hopmans, E.C., Cohen, A.S., 2008. Northern hemisphere controls on tropical southeast African climate during the past 60,000 years. Science 84 322, 252–255. https://doi.org/10.1126/science.1160485.
Tierney, J.E., Russell, J.M., Huang, Y., 2010. A molecular perspective on Late Quaternary climate and vegetation change in the Lake Tanganyika basin, East Africa. Quat. Sci. Rev. 29, 787–800. https://doi.org/10.1016/j.quascirev.2009.11.030.
Tierney, J.E., Lewis, S.C., Cook, B.I., LeGrande, A.N., Schmidt, G.A., 2011a. Model, proxy and isotopic perspectives on the East African Humid Period. Earth Planet Sci. Lett. 307, 103–112. https://doi.org/10.1016/j.epsl.2011.04.038.
Tierney, J.E., Russell, J.M., Sinninghe Damsté, J.S., Huang, Y., Verschuren, D., 2011b. Late quaternary behavior of the East African monsoon and the importance of the Congo air boundary. Quat. Sci. Rev. 30, 798–807. https://doi.org/10.1016/j.quascirev.2011.01.017.
Tierney, J.E., Pausata, F.S.R., De Menocal, P.B., 2017. Rainfall regimes of the green Sahara. Sci. Adv. 3, 1–10. https://doi.org/10.1126/sciadv.1601503.
Tipple, B.J., Berke, M. a, Doman, C.E., Khachaturyan, S., Ehleringer, J.R., 2013. Leaf-wax n-alkanes record the plant-water environment at leaf flush. Proc. Natl. Acad. Sci. U.S.A. 110, 2659–2664. https://doi.org/10.1073/pnas.1213875110.
Urban, M.A., Nelson, D.M., Street-Perrott, F.A., Verschuren, D., Hu, F.S., 2015. A late-Quaternary perspective on atmospheric pCO2, climate, and fire as drivers of C4-grass abundance. Ecology 96, 642–653. https://doi.org/10.1890/14-0209.1.
Vachula, R.S., Richter, N., 2017. Informing sedimentary charcoal-based fire reconstructions with a kinematic transport model. Holocene 28, 173–178.
Vachula, R.S., Karp, A.T., Denis, E.H., Balascio, N.L., Canuel, E.A., Huang, Y., 2022. Spatially calibrating polycyclic aromatic hydrocarbons (PAHs) as proxies of area burned by vegetation fires: insights from comparisons of historical data and sedimentary PAH fluxes. Palaeogeogr. Palaeoclimatol. Palaeoecol. 596, 110995. https://doi.org/10.1016/j.palaeo.2022.110995.
van Bree, L.G.J., Peterse, F., van der Meer, M.T.J., Middelburg, J.J., Negash, A.M.D., De Crop, W., Cocquyt, C., Wieringa, J.J., Verschuren, D., Sinninghe Damsté, J.S., 2018. Seasonal variability in the abundance and stable carbon-isotopic composition of lipid biomarkers in suspended particulate matter from a stratified equatorial lake (Lake Chala, Kenya/Tanzania): implications for the sedimentary record. Quat. Sci. Rev. 192, 208–224. https://doi.org/10.1016/j.quascirev.2018.05.023.
Van Der Werf, G.R., Randerson, J.T., Giglio, L., Gobron, N., Dolman, A.J., 2008. Climate controls on the variability of fires in the tropics and subtropics. Global Biogeochem. Cycles 22, 1–13. https://doi.org/10.1029/2007GB003122.
Van Der Werf, G.R., Randerson, J.T., Giglio, L., Van Leeuwen, T.T., Chen, Y., Rogers, B.M., Mu, M., Van Marle, M.J.E., Morton, D.C., Collatz, G.J., Yokelson, R.J., Kasibhatla, P.S., 2017. Global fire emissions estimates during 1997-2016. Earth Syst. Sci. Data 9, 697–720. https://doi.org/10.5194/essd-9-697-2017.
van Geel, B., Gelorini, V., Lyaruu, A., Aptroot, A., Rucina, S., Marchant, R., Damsté, J.S.S., Verschuren, D., 2011. Diversity and ecology of tropical African fungal spores from a 25,000-year palaeoenvironmental record in southeastern Kenya. Rev. Palaeobot. Palynol. 164, 174–190. https://doi.org/10.1016/j.revpalbo.2011.01.002.
Van Marle, M.J.E., Kloster, S., Magi, B.I., Marlon, J.R., Daniau, A.L., Field, R.D., Arneth, A., Forrest, M., Hantson, S., Kehrwald, N.M., Knorr, W., Lasslop, G., Li, F., Mangeon, S., Yue, C., Kaiser, J.W., Van Der Werf, G.R., 2017. Historic global biomass burning emissions for CMIP6 (BB4CMIP) based on merging satellite observations with proxies and fire models (1750-2015). Geosci. Model Dev. (GMD) 10, 3329–3357. https://doi.org/10.5194/gmd-10-3329-2017.
Verschuren, D., Sinninghe Damsté, J.S., Moernaut, J., Kristen, I., Blaauw, M., Fagot, M., Haug, G.H., 2009. Half-precessional dynamics of monsoon rainfall near the East African Equator. Nature 462, 637–641. https://doi.org/10.1038/nature08520.
Vincens, A., Chalié, F., Bonnefille, R., 1993. Pollen-derived rainfall and temperature estimats from Lake Tanganyika and their implication for lakee Pleistocene water levels. Quat. Res. 40, 343–350.
Wakeham, S.G., Pease, T.K., 2004. Lipid Analysis in Marine Particle and Sediment Samples.
Wakeham, S.G., Schaffner, C., Giger, W., 1980. Polycyclic aromatic hydrocarbons in recent lake sediments—I. Compounds having anthropogenic origins. Geochem. Cosmochim. Acta 44, 403–413. https://doi.org/10.1016/0016-7037(80)90040-X.
Waldram, M.S., Bond, W.J., Stock, W.D., 2008. Ecological engineering by a mega-grazer: white Rhino impacts on a south African savanna. Ecosystems 11, 101–112. https://doi.org/10.1007/s10021-007-9109-9.
Yunker, M.B., Macdonald, R.W., Vingarzan, R., Mitchell, R.H., Goyette, D., Sylvestre, S., 2002. PAHs in the Fraser River basin: a critical appraisal of PAH ratios as indicators of PAH source and composition. Org. Geochem. 33, 489–515. https://doi.org/10.1016/S0146-6380(02)00002-5.
Yuretich, R.F., 1986. Controls on the composition of modern sediments, Lake Turkana, Kenya. Geol. Soc. Spec. Publ. 25, 141–152. https://doi.org/10.1144/GSL.SP.1986.025.01.12.